# THE HYPERFINE STRUCTURE OF SAMARIUM-153 AND SAMARIUM-155

# A STUDY OF THE HYPERFINE STRUCTURE

# OF

# SAMARIUM-153 AND SAMARIUM-155

By

HAROLD KEITH EASTWOOD, B.Sc.

A Thesis

Submitted to the Faculty of Graduate Studies

in Partial Fulfilment of the Requirements

for the Degree

Doctor of Philosophy

McMaster University

May 1964

DOCTOR OF PHILOSOPHY (1964)
(Physics)

McMASTER UNIVERSITY
Hamilton, Ontario.

TITLE: A Study of the Hyperfine Structure of Samarium-153 and Samarium-155

AUTHOR: Harold Keith Eastwood, B.Sc. (McMaster University)

SUPERVISOR: Dr. R. G. Summers-Gill

NUMBER OF PAGES: ix, 94

SCOPE AND CONTENTS:

It was the purpose of this investigation to study the hyperfine structure of the β-unstable isotopes of samarium using the atomic beam magnetic resonance technique. A brief review is given of the nuclear and atomic theory necessary for the interpretation of the experiments.

The hyperfine interaction constants (Mc/sec) for $Sm^{153}$, and the nuclear moments inferred from them, are summarized below:

| | | |
|---|---|---|
| $A_1 = -2.100(5)$ | $B_1 = 289.042(4)$ | |
| $A_2 = -2.573(6)$ | $B_2 = 306.521(21)$ | $C_2 = -0.0003(9)$ |
| $A_3 = -3.115(4)$ | $B_3 = 165.824(20)$ | $C_3 = -0.0087(12)$ |
| $\mu_I = -0.021(1)$ n.m. | $Q = 1.1(3)$ barns | |

From the quadrupole moment it follows that the nuclear deformation $\delta = 0.25(5)$. The magnetic moment disagrees with the predictions of the Nilsson model for either spin 3/2 state with which the $Sm^{153}$ ground state might be associated.

Also determined was the spin of $Sm^{155}$. The result, $I = 3/2$, confirms the assignment from the less direct evidence available from radioactive decay studies. The more extensive measurements necessary to determine the moments were not attempted.

ACKNOWLEDGEMENTS

I would like to express my appreciation to all those who made this research possible.

To the Faculty of McMaster University who contributed to my education first as an undergraduate and later as a graduate student.

To Dr. R. G. Summers-Gill for suggesting this problem, for his invaluable aid with the computations, and especially for his unfailing interest.

To Dr. H. J. King and Dr. J. A. Cameron, two former members of the atomic beam group, who as graduate students worked on the design and construction of the atomic beam apparatus.

To G. M. Stinson and other members of the atomic beam group for their able assistance in performing the experiments which necessitated many hours of cooperative effort.

To Dr. G. K. Woodgate of the Clarendon Laboratories for supplying the data on $Sm^{147}$ and $Sm^{149}$ prior to publication.

To the staff of the reactor and of the machine shop and many others for their valuable assistance.

To my parents for their encouragement.

Finally, to my wife, Donalda, who has endured five long years as a graduate student's wife, performing the duties of housewife, breadwinner and mother of our two children.

The author would like to acknowledge the financial assistance received from the Department of Physics. This research was supported by grants-in-aid from the National Research Council.

TABLE OF CONTENTS

LIST OF FIGURES

## LIST OF TABLES

# CHAPTER I. INTRODUCTION

Historically, the first applications of atomic beams to the study of atomic structure were the experiments of Stern and Gerlach which proved the space quantization of the electronic magnetic moment (Gerlach and Stern, 1921). These simple deflection experiments developed into the so-called zero-moment method for measuring nuclear spins. Values of magnetic moments obtained by this method were little more than estimates. In 1938, Rabi introduced atomic beam magnetic resonance (Rabi et al., 1938). This new technique, specifically designed for accurate measurements of the properties of low-lying states of free atoms, permits the determination of the spectroscopic splitting factor $g_J$ with a precision unequalled by any other method. Also, in cases where the atomic spectrum is too complex to yield an unambiguous ground state assignment, this can often be made by atomic beam magnetic resonance. Recently, this method was used successfully in the rare earth and transuranic regions.

The properties of the nuclear ground state can also be inferred from radio-frequency investigations of the atomic hyperfine structure. Thus atomic beam experiments are a prime source of nuclear data, particularly since the method may also be applied to the study of radioactive nuclides (Bellamy and Smith, 1953). The measured values of nuclear spin and multipole moments can be used to test the validity of theories of nuclear structure. The strongest experimental support for the shell theory of the nucleus came from the observed values of

spin. Similarly the large values of quadrupole moment of certain nuclei were important in the development of the collective model. A contribution of fundamental significance was the observation of the quadrupole moment of the deuteron (Kellogg et al., 1939) and the consequent inference of the tensor part of the internucleon force (Rarita and Schwinger, 1941).

Most investigations cannot compare with the latter experiment in importance. However, there are several regions of the nuclidic chart where systematic variations in nuclear structure can be elucidated by the measurement of nuclear moments. The two different models mentioned above, the shell model and the collective model, are widely and successfully applied in different mass regions. The transitions between areas where these models are applicable are of particular interest. One such transition occurs for neutron numbers between 85 and 90 and the samarium isotopes were chosen for this investigation because they illustrate this change. The excited states of ${}_{62}Sm^{152}_{90}$ show rather well developed rotational structure, characteristic of deformed nuclei. In the lighter even-even isotopes of samarium, the low-lying states are more typical of spherical nuclei. The level structures of the odd isotopes $Sm^{149}$ and $Sm^{151}$ are very complex. Although there have been several recent studies of the levels of $Sm^{151}$ a detailed interpretation awaits the measurement of its ground state spin (Burke et al., 1963; Harmatz et al., 1962).

The isotopes $Sm^{147}$ and $Sm^{149}$ have been investigated by the atomic beam technique (Woodgate, 1963). The spins can be accounted for by the shell model and the relatively small quadrupole moments also imply that the nuclei are basically spherical. The spin of $Sm^{153}$ has also been

measured (Cabezas *et al.*, 1960) and this can be interpreted in terms of the collective model. By extending these measurements it is intended to bridge this transition from shell model to collective model.

## CHAPTER II. NUCLEAR MOMENTS

The electromagnetic properties of the nucleus arise from the charge and current density of an assembly of nucleons. The charge on the nucleus is the sum of the charge on the individual protons Ze while the current density is made up of two contributions: the proton currents and the currents associated with the nucleon spins. If one is considering the interaction of the nucleus with an external electromagnetic system, e.g. the atomic electrons, it is convenient to expand the interaction in terms of the multipole moments. Thus the energy of interaction can be written as a sum of terms proportional to the nuclear moments; monopole, dipole, quadrupole, etc. If the distance between the two systems is large compared to the nuclear dimensions, then these terms diminish rapidly in size and the series can be terminated with only a few terms.

The electric and magnetic multipole operators of order $\lambda$ are:

$$Q_\lambda^\mu = e \sum_{K=1}^{Z} r_K^\lambda \, Y_\lambda^\mu(\theta_K) \tag{1}$$

$$M_\lambda^\mu = \mu_N \sum_{K=1}^{A} \nabla(r_K^\lambda \, Y_\lambda^\mu(\theta_K)) \cdot \left[ g_\ell \frac{2\ell_K}{\lambda+1} + g_s s_K \right]$$

where $r_K$, $\theta_K$, $\phi_K$ are the coordinates of the $k^{th}$ nucleon, $Y_\lambda^\mu(\theta_K)$ is a spherical tensor or order $\lambda$ and projection $\mu$, and $g_\ell$ and $g_s$ are the orbital and spin gyromagnetic ratios. The electronic charge is e and $\mu_N$ is the nuclear magneton. Several restrictions apply to the observable operators because of the properties of the spherical tensors. Because

$Y_\lambda^\mu(\theta_K)$ has parity $(-1)^\lambda$ it follows that $Q_\lambda^\mu$ and $M_\lambda^\mu$ have parities $(-1)^\lambda$ and $(-1)^{\lambda+1}$, respectively. Since odd parity operators have zero expectation value in states of definite parity, the only static multipole moments are the even electric moments and the odd magnetic moments. The odd parity operators are important, however, in determining the electromagnetic transitions between nuclear states of different parity. The expectation value of the spherical tensor operator $Q_\lambda^\mu$ can be evaluated in the nuclear state $|IM\rangle$ by the Wigner-Eckart theorem:

$$\langle IM' | Q_\lambda^\mu | IM \rangle = (I\ \lambda\ M\ \mu | IM')\ \langle I \| Q_\lambda^\mu \| I \rangle$$

The Clebsch-Gordan coefficient vanishes unless $\underline{I}$ and $\underline{\lambda}$ add vectorally to form $\underline{I}$ (i.e. $\lambda \leqslant 2I$). Thus the highest order static electric multipole with non-zero expectation value is the $2^{2I}$ pole. The same restriction applies to $M_\lambda^\mu$.

It would be difficult to evaluate equation (1) with all the degrees of freedom for any but the simplest nuclei; hence we must resort to simplifying models. These models should be consistent with our knowledge of internucleon forces and the known properties of nuclei. On the basis of the accumulated nuclear data, two general features stand out. First, certain numbers of nucleons show particular stability as reflected in nucleon binding energies and in the abundance of stable nuclei with " magic numbers" of neutrons or protons. Second, the nuclei in certain regions ($A \sim 25$, $150 < A < 190$ and $A > 225$) have a well developed rotational band structure. This suggests that the equilibrium shapes of nuclei in these regions are spheroidal. Two types of models which were developed to account for these features are discussed below.

## 1. Single Particle Models

The basis of the single particle model is the assumption that a static potential well can be used to represent the average internucleon forces. The usefulness of this model was not recognized until a term in the potential, proportional to the product of the nucleon spin and orbital angular momentum, was added (Mayer, 1948; Haxel et al, 1948). The strengths of the two interactions are adjusted to fit the observed sequence of energy levels and, with reasonable values, will give energy gaps at the "magic numbers". The resultant energy states fill separately with neutrons and protons in accordance with the Pauli principle. To be consistent with the observation that even-even nuclei have spin zero, it is assumed that the angular momenta of an even number of like particles, in the same state, couple to give zero resultant.

For odd-A nuclei, the extreme single particle model assumes that most of the nuclear properties are due to the odd nucleon outside an even-even core. Thus the nuclear spin is the vector sum of the spin s and orbital angular momentum $\ell$ of this particle and the parity of the nuclear state is the same as that of the single particle state.

For odd-odd nuclei, there is some ambiguity as to the way in which the proton and neutron angular momenta should couple. Empirical coupling schemes have been suggested which are reasonably successful at predicting the ground state spins for odd-odd nuclei (Nordheim, 1951; Brennan and Bernstein, 1960).

The magnetic moment due to the unpaired nucleon in state $|n\ell j\rangle$ is:

$$\mu_{sp} = \frac{1}{2} j \left[ (g_\ell + g_s) + (g_\ell - g_s) \frac{\ell(\ell + 1) - 3/4}{j(j + 1)} \right] \qquad (2)$$

where $j = \ell \pm 1/2$ is the total angular momentum of the odd nucleon. The limiting Schmidt moments are obtained by using the free nucleon values for $g_\ell$ and $g_s$ (Schmidt, 1937):

| | Neutron | Proton |
|---|---|---|
| Orbital gyromagnetic ratio $g_\ell$ | 0 | 1 |
| Free particle spin gyromagnetic ratio $g_s$ | - 3.826 | 5.586 |

Experimentally-determined magnetic moments are found to lie generally between the Schmidt values, but it is usually possible to assign the parity of a nucleus by associating the moment with the nearer of the two limits. One can get better agreement between the model and experiment by reducing the free nucleon gyromagnetic ratio $g_s$ towards the Dirac values. Although one might expect quenching of the free moments in nuclear matter, quantitative corrections are not possible at the present state of meson theory.

Since there is no contribution from the spherical core, the extreme single particle model predicts a nuclear quadrupole moment due only to the odd proton; namely,

$$Q_{sp} = - \frac{e^2(2j - 1)}{2(j + 1)} \left\langle r^2 \right\rangle_j \tag{3}$$

The expectation value of the square of the radial coordinate of the proton $\left\langle r^2 \right\rangle_j$ can be approximated by $3/5 R_n^2 \approx A^{2/3} \times 10^{-26}$ cm$^2$ where $R_n$ is the nuclear radius. For an odd neutron nucleus there is no intrinsic moment but the recoil of the charged core contributes a value:

$$Q_{sn} = \frac{Z}{A^2} Q_{sp} \tag{4}$$

These predictions differ seriously from the observed moments. Whereas the model predicts only negative quadrupole moments, the observed values are

nearly all positive. The quadrupole moments show no such simple variation with A and are generally much larger than predicted, particularly for the region of deformed nuclei. Finally, the observed quadrupole moments of odd-N nuclei are as large, on the average, as the moments of odd-Z nuclei.

In summary, although the extreme single particle model can predict ground state spins and parities, it is less successful predicting the values of magnetic and quadrupole moments. Clearly it does not take adequate account of the inter-nucleon forces.

In the more realistic single particle model, it is assumed that only nucleons in completely filled energy levels couple to spin zero. The interaction of the nucleons outside this core is separated into a mean particle-core interaction, a particle spin-orbit interaction and a residual particle-particle interaction. If it is assumed that this residual interaction is small compared to the effective single particle force, it can be treated as a perturbation and the single particle wave functions can be used as a basis for "configuration mixing" calculations. The result of the interaction is to mix states of the same parity and orbital angular momentum, particularly the components of the spin-orbit doublet. The nuclear magnetic moment can be extremely sensitive to small admixtures of certain configurations and it is possible to account for the deviation from the Schmidt values qualitatively (Blin-Stoyle, 1957; Arima and Horie, 1954).

The individual particle model is an even more comprehensive attempt at expressing nucleon properties in terms of the single particle states. The basis of this model is to first form a set of anti-symmetrical wave functions which are as realistic as possible. These are

then used as a representation in which to diagonalize the energy matrix. The lowest lying energy levels are selected using the concepts of isotopic spin and seniority. Because of the difficulty of this procedure, it has been carried out only for light nuclei with relatively simple interactions, i.e. a central potential with spin-orbit coupling (Kurath, 1956; Elliot and Flowers, 1955). In the limited range ($A < 40$) for which calculations have been made, this model is quite successful.

2. The Collective Model

The foregoing models fail to account for the regularly spaced energy states of many even-even nuclei. For $150 < A < 190$ and $A > 225$, the regular spacing of these energy levels is suggestive of the rotational band structure of diatomic molecules. In several other mass regions, the energy levels are nearly equally spaced, akin to molecular vibrational spectra. When these observations are supported by the large experimental quadrupole moments of these nuclei and the high electric quadrupole transition probabilities, it is clear that these effects can only arise from the cooperative effect of many nucleons. This correlation may come about through a long-range residual inter-nucleon force which couples the individual particle motions to the motion of the nuclear surface.

In the collective model the long-range correlation is accounted for by assuming a shell model potential which is, in general, spheroidal rather than spherical (Bohr and Mottelson, 1953; Nilsson, 1955). The energy of particle states is calculated as a function of deformation. The properties of this model are considered in the case of weak and strong coupling of particles to the core.

For weak coupling, the deformation is small and the equilibrium nuclear shape is nearly spherical. The particle surface interaction can be treated by perturbation theory and has the effect of mixing, into the

particle states, nearby states of the same parity differing by no more than two units of angular momentum. In this limit the model is essentially the same as the shell model with configuration mixing.

For strong coupling, the Hamiltonian can be separated into parts describing the rotational and vibrational degrees of freedom and the particle excitation, analogous to the linear molecule. Nilsson has calculated the wave functions for an axially-symmetric potential. They are linear combinations of the solutions of the spherical harmonic oscillator. In his notation this is written:

$$\Psi_{\delta\ell} = \sum \alpha_{\ell\Omega}(\delta) \, | N\ell\Lambda\Sigma \rangle$$

where N is the total oscillator quantum number and $\Lambda$ and $\Sigma$ are the projections on the symmetry axis of the particle angular momenta $\ell$ and s. If one writes $\underline{\Omega} = \underline{\Lambda} + \underline{\Sigma}$, then the nuclear spin $\underline{I} = \underline{R} + \underline{\Omega}$ where R is the angular momentum of the core. Since R = 0 in the ground state, $I = \Omega = \Lambda + \Sigma$. In the limit of extreme deformation, the spin-orbit term may be treated as a perturbation, and then the quantum numbers are $| N \, n_z \Lambda \rangle$ where $n_z$ is the projection of N on the symmetry axis. The Nilsson energy levels are labelled by these asymptotic quantum numbers.

The nuclear magnetic dipole moment can be evaluated using the Nilsson mixing coefficients. For $I \neq 1/2$

$$\mu = \frac{I}{I+1}\left[g_\ell I + g_R + 1/2(g_s - g_\ell)\sum\left(a^2_{\ell\,\Omega-1/2}(\delta) - a^2_{\ell\,\Omega+1/2}(\delta)\right)\right] \qquad (5)$$

The expansion is slightly more complicated for I = 1/2 since there is now no direct particle-surface coupling. The gyromagnetic ratio $g_R$ takes account of the dipole moment due to the collective rotation of the core. For a uniform charge distribution $g_R \approx \frac{Z}{A}$. Experimental values of $g_R$ can be obtained from the magnetic moments of the first rotational states of

even-even nuclei (Goldring and Scharenberg, 1958; Manning and Rogers, 1960). Their values are about $\frac{Z}{2A}$ and it seems probable that this discrepancy is due to the difference in size of the neutron and proton distributions.

The intrinsic quadrupole moment $Q_o$ is related to the deformation $\delta$. If one neglects the small contribution of the single particle and assumes a uniform charge density then

$$Q_o = \frac{4}{5} \delta \, Z \, R_o^2 (1 + 1/2 \, \delta + \cdots) \tag{6}$$

where $R_o \approx 1.2 \times 10^{-13} A^{1/3}$ is the mean radius of the charge distribution. In an experiment, such as an atomic beam investigation, the measured value of the quadrupole moment will be the projection of $Q_o$ on a space fixed axis.

$$Q = Q_o \frac{I(2I - 1)}{(I + 1)(2I + 3)} \tag{7}$$

The intrinsic quadrupole moment can also be derived from a study of the quadrupole transition probabilities in Coulomb excitation and $\gamma$-decay of the excited rotational levels of these nuclei.

Although the collective model gives reasonable agreement with experiment for the deformed nucleus, it does not give an adequate description of the transition between weak and strong coupling. One might expect the coupling to increase gradually as the number of loosely bound nucleons in a shell is increased. Experimentally, the change is abrupt and occurs within a few mass numbers.

This effect can be explained by adding an additional short range pairing force which couples pairs of nucleons identical except for their spin projection. The concept of these "quasi-particle" pairs and the theoretical treatment is analogous to the analysis of superconductivity

(Bardeen, Cooper and Schreifer, 1957). The pairing energy favours a spherical configuration, whereas the long range quadrupole energy favours a strongly deformed nucleus and it can be shown (Bilyaev, 1959) that a small change in the number of particles in the unfilled shell will cause an abrupt change in the equilibrium deformation.

This treatment of the pairing force has also been applied to the single particle shell model by Kisslinger and others (Kisslinger and Sorensen, 1960; Kisslinger and Freed, 1961). Nuclear magnetic moments calculated in this way are in good agreement with the experimental values. Of course the calculations were only made in regions where the spherical model is applicable. There is hope that a unified model including long range correlations, pairing interaction, and single particle effects will be capable of explaining the detailed properties of nuclei in all mass regions.

## CHAPTER III. THEORY OF HYPERFINE STRUCTURE

### 1. Atomic Hamiltonian

In the absence of any external interaction, the atomic Hamiltonian may be written as

$$\mathcal{H}_{\text{atomic}} = \mathcal{H}_{\text{nuclear}} + \mathcal{H}_{\text{electronic}} + \mathcal{H}_{\text{hyperfine}} . \qquad (8)$$

The first term, $\mathcal{H}_{\text{nuclear}}$, represents the internal energy of the nucleus. The nuclear energy levels are widely spaced, compared to the electronic energy levels involved in optical and hyperfine transitions. Thus, the nucleus can be considered to be in a single eigenstate characterized by nuclear spin I and this term will be omitted in further consideration. The second term, $\mathcal{H}_{\text{electronic}}$, describes the interaction of Z electrons moving in the central Coulomb field of a point nucleus with charge Ze. We can write:

$$\mathcal{H}_{EL} = \sum_{i=1}^{Z} \left[ \frac{P_i^2}{2m} - \frac{Ze^2}{r_i} + \frac{1}{2} \sum_{j \neq i} \frac{e^2}{r_{ij}} + \xi(r_i) \underline{\ell}_i \cdot \underline{s}_i \right] . \qquad (9)$$

This Hamiltonian, summed over the Z electrons, has the usual electron kinetic energy term, the electrostatic interaction with the nucleus and with the remaining electrons and a spin-orbit magnetic interaction. One might have also included a more general spin-orbit term ($\underline{\ell}_i \cdot \underline{s}_j$) but this appears to be negligibly small. It is impractical to solve the wave equation for this Hamiltonian directly; instead it is treated by perturbation theory. Write an approximate Hamiltonian,

$$\mathcal{H}_o = \sum_i \left[ \frac{P_i^2}{2m} + V(r_i) \right]$$

where $V(r_i)$ is a spherically symmetric potential which approximates the potential at the position of the $i^{th}$ electron. Solution of the wave equation then yields product wave functions of the individual electrons. These highly degenerate hydrogenic wave functions, anti-symmetrized to conform to the Pauli principle, can serve as a basis for perturbation theory calculations. The eigenstates, labelled by the principle quantum numbers $n_i$ and orbital angular momenta $\ell_i$, characterize the gross structure of the atom. The remaining interactions are treated as perturbations in this Hamiltonian:

$$\mathcal{H}_{Pert} = \mathcal{H}_{EL} - \mathcal{H}_o = \sum_i \left[ \frac{1}{2} \sum_{j \neq i} \frac{e^2}{r_{ij}} - \frac{Ze^2}{r_i} - V(r_i) \right] + \sum_i \xi(r_i) \underline{\ell}_i \cdot \underline{s}_i \, .$$

The treatment of $\mathcal{H}_{Pert}$ depends on the relative size of the first and second terms. If the electrostatic term dominates, as is usually the case for the lighter atoms, then the total angular momentum L and the total spin S are good quantum numbers (Russell-Saunders coupling). In this case, the spin-orbit term acts as a further perturbation, splitting each term into fine structure levels characterized by different values of $\underline{J} = \underline{L} + \underline{S}$. For a given configuration, the state with the greatest total spin S will lie lowest. This aspect of Hund's rule arises from the dependence of the electrostatic interaction on the symmetry of the wave function.

In the case of heavier atoms, the fine structure interaction is the same order as the electrostatic term, so that L and S are no longer good quantum numbers. If the spin-orbit term dominates then the electron angular momenta $\ell_i$ and $s_i$ couple to form the individual electron total

angular momentum $j_i$. The degeneracy of the states in this representation, characterized by $\underline{J} = \Sigma\, \underline{j_i}$, is removed by the perturbation of the residual electrostatic interaction.

The smallest and final term in equation (8) arises from the electric and magnetic interactions between the nucleus and electronic system, excluding the point charge Coulomb interaction. This interaction splits each fine structure level into 2X + 1 hyperfine levels, each of total angular momentum $\underline{F} = \underline{I} + \underline{J}$ (X = the smaller of the electronic angular momentum J or nuclear spin I). The rest of this chapter will be concerned with $\mathcal{H}_{HF}$ and, since L-S coupling appears to be approximately valid for samarium in the ground state term, we will consider the atom to be in a state denoted by the quantum numbers L, S, J and I.

2. Hyperfine Interaction

Since 1924, when Pauli postulated that hyperfine structure arises from the interaction of the angular momentum of the nucleus with the electronic system, there have been several theoretical treatments of this subject (Goudsmit, 1931; Breit and Wills, 1933; Casimir, 1936; Schwartz, 1955). In the preceeding chapter the nuclear multipole operators were written as spherical tensors. The multipole operators of the electronic system can be expressed similarly. Schwartz shows that the hyperfine interaction can be represented by the contraction of these spherical tensors.

$$\mathcal{H}_{HF} = \sum_{\lambda} \sum_{\mu} (-1)^{\mu}\, Q_{\lambda}^{\mu}(e)\, Q_{\lambda}^{-\mu}(n)$$

$$= \sum_{\lambda} Q_{\lambda}(e) \cdot Q_{\lambda}(n) \qquad (10)$$

$Q_{\lambda}(e)$ is a reduced tensor operator of the electron multipole expansion. Since only even electric and odd magnetic static multipole operators have

non-zero expectation values, the same symbol $Q_\lambda$ is used to represent either type depending on whether $\lambda$ is even or odd. In order to express the expectation value of the hyperfine Hamiltonian in the state $|I\ J\ F\ m\rangle$ where m is the projection of F on the quantization axis, one writes:

$$W_{Fm} = \langle I\ J\ F\ m|\mathcal{H}_{HF}|I\ J\ F\ m\rangle$$

$$= \sum_\lambda \langle I\ J\ F\ m|Q_\lambda(e)\cdot Q_\lambda(n)|I\ J\ F\ m\rangle \qquad (11)$$

Evaluating each term separately, using a theorem due to Racah, gives

$$W_{Fm}(\lambda) = (-1)^{I+J-F}\begin{Bmatrix} F & J & I \\ \lambda & I & J \end{Bmatrix}\langle I\|Q_\lambda(n)\|I\rangle\langle J\|Q\lambda(e)\|J\rangle$$

The symbol in the brackets is the Wigner 6 - j symbol and the last two factors are reduced matrix elements of the spherical tensors. One notes that the terms are independent of the magnetic quantum number m and thus can be written as $W_F(\lambda)$. On expanding the Wigner 6 - j symbol, the first three terms of the multipole expansion are (Alpert, 1961):

$$W_F(1) = \frac{\mathcal{A}_1 D}{2IJ}$$

$$W_F(2) = \frac{3\,\mathcal{A}_2\left[D(D+1) - \frac{4}{3}I(I+1)J(J+1)\right]}{2I(2I-1)J(2J-1)}$$

$$W_F(3) = \frac{5\,\mathcal{A}_3\left[D^3+4D^2-\frac{4}{3}D\left\{-3I(I+1)J(J+1)+I(I+1)+3\right\} - 4I(I+1)J(J+1)\right]}{4I\,(I-1)(2I-1)J(J-1)(2J-1)}$$

(12)

where $D = F(F+1) - I(I+1) - J(J+1)$.

The commonly used hyperfine structure constants a, b anc c, which have the dimensions of frequency, are defined by

$$\mathcal{A}_1 = I\,J\,h\,a$$

$$\mathcal{A}_2 = h\,b\,/\,4$$

$$\mathcal{A}_3 = h\,c$$

The total hyperfine energy can then be written

$$W_F = \frac{haD}{2} + \frac{3}{8} hb \frac{\left[D(D+1) - \frac{4}{3} I(I+1)J(J+1)\right]}{I(2I-1)J(J-1)}$$

$$+ \frac{5}{4} hc \frac{\left[D^3 + 4D^2 - \frac{4}{3}D\left\{-3I(I+1)J(J+1) + I(I+1) + 3\right\} - 4I(I+1)J(J+1)\right]}{I(I-1)(2I-1)J(J-1)(2J-1)}$$

$$+ \text{higher terms.} \tag{13}$$

Neglecting all but the first two terms, Baker, of the atom beam group at the University of California, Berkeley, has computed extensive tables showing the dependence of the hyperfine level ordering and spacing on a and b for various I and J (Baker, 1960).

In calculating $W_F$ we have considered J to be a good quantum number. However, neighbouring electronic levels perturb the hyperfine states giving rise to terms, off diagonal in J, of order $\Delta W_F^2/\Delta W_{EL}$. This effect is not negligible for states with large hyperfine separation $\Delta W_F^2$ and small fine structure separation $\Delta W_{EL}$, but the specific form of the corrections is available only for single electron atoms (Schwartz, 1955).

The values of the interaction constants depend explicitly on the nuclear moments and on the electronic wave function. For atoms with a single valence electron, the expressions for a, b anc c are given in several references (e.g. Ramsey, 1956). General expressions for higher order interactions have been published by Schwartz, but their effect has not been observed. The hyperfine constants for multi-electron configurations, represented by capital letters, depend on the form of electron coupling, j-j, intermediate, or L-S. In the case of L-S coupling of non-s electrons to give the Hund's rule ground state term, these take the form (Hubbs <u>et al</u>, 1958; Winocur, 1960):

$$A = \frac{\mu_I \mu_o}{hIJ(J+1)} \sum_{\ell} \left\langle \frac{1}{r^3} \right\rangle_{\ell n_\ell} \left[ -K \frac{(2\ell - n_\ell + 1)}{2L} \pm \frac{n_\ell (2\ell - n_\ell + 1)(2\ell - 2n_\ell + 1)}{2LS(2L-1)(2\ell+3)(2\ell-1)} \right.$$

$$\left. \left\{ L(L+1) \left[ J(J+1) + S(S+1) - L(L+1) \right] + \frac{3}{2} K \left[ J(J+1) - L(L+1) - S(S+1) \right] \right\} \right]$$

$$B = \frac{e^2 Q}{h} \left[ \frac{3K(K+1) - 4L(L+1)J(J+1)}{2L(2L-1)(J+1)(2J+3)} \right] \sum_{\ell} (\pm 1) \left\langle \frac{1}{r^3} \right\rangle_{\ell n_\ell} \frac{n_\ell (2\ell - n_\ell + 1)(2\ell - 2n_\ell + 1)}{(2\ell+3)(2\ell-1)} \tag{14}$$

where $S = \frac{1}{2} \sum_{\ell} n_\ell$, $L = \frac{1}{2} \sum_{\ell} n_\ell (2\ell - n_\ell + 1)$ and $K = S(S+1) - L(L+1) - J(J+1)$ and $n_\ell$ is the number of electrons (holes) in the $\ell$ orbital. The sums are taken over all partially filled orbitals and the plus sign is used for shells less than half filled and the negative sign for shells more than half filled.

3. Magnetic Interaction

In the preceding section, we have considered only the interactions within a free atom. In the presence of an external magnetic field $\underline{H}$, a term must be added to the hyperfine Hamiltonian describing the interaction of the electronic and nuclear magnetic moments with the field. Thus the total Hamiltonian becomes

$$\mathcal{H}_T = \mathcal{H}_{HF} + \mathcal{H}_{MAG}$$

where

$$\mathcal{H}_{MAG} = -\underline{\mu_J} \cdot \underline{H} - \underline{\mu_I} \cdot \underline{H}$$

$\underline{\mu_J} = + g_J \mu_o \underline{J}$ is the electronic magnetic moment and $\underline{\mu_I} = +g_I \mu_o \underline{I}$ is the nuclear magnetic moment. Since the electron magnetic moment is anti-parallel to its angular momentum, $g_J$ always has a negative value. The literature is not consistent in this respect. Note that the nuclear gyro-magnetic ratio $g_I$ is defined here in units of the Bohr magneton $\mu_o = \frac{e\hbar}{2mc}$,

whereas, in Chapter II, it was in units of the nuclear magneton

$\mu_N = \frac{eh}{2Mc} \approx \frac{\mu_o}{2000}$ .

If the magnetic field is in the z direction,

$$\mathcal{H}_{MAG} = - g_J \mu_o J_z H - g_I \mu_o I_z H . \tag{15}$$

Although this operator is diagonal in the $|I\ J\ m_I m_J\rangle$ representation, $\mathcal{H}_{HF}$ is not. Conversely, in the $|I\ J\ F\ m\rangle$ representation, $\mathcal{H}_{HF}$ is diagonal and $\mathcal{H}_{MAG}$ is not -- in fact, there will be matrix elements connecting states for which F differs by $\pm 1$. If the magnetic interaction is small compared to $\mathcal{H}_{HF}$, then, by perturbation theory,

$$\begin{aligned} W_{Fm} &= \langle Fm|\mathcal{H}_T|Fm\rangle \\ &= \langle Fm|\mathcal{H}_{HF}|Fm\rangle + \langle Fm|\mathcal{H}_{MAG}|Fm\rangle \\ &\quad + \sum_{F \neq F'} \frac{\langle Fm|\mathcal{H}_{MAG}|F'm'\rangle^2}{W_F - W_{F'}} + \text{higher order terms} \end{aligned} \tag{16}$$

where $W_F = \langle Fm|\mathcal{H}_{HF}|Fm\rangle$ is given by equation (13). Only three matrix elements of $\mathcal{H}_{MAG}$ are non-vanishing

$$\langle Fm|\mathcal{H}_{MAG}|Fm\rangle = - m \left[ g_J \mu_o H \frac{F(F+1)+J(J+1)-I(I+1)}{2F(F+1)} + g_I \mu_o H \frac{F(F+1)+I(I+1)-J(J+1)}{2F(F+1)} \right]$$

$$\begin{aligned} \langle Fm|\mathcal{H}_{MAG}|F-1m\rangle &= \langle F-1m|\mathcal{H}_{MAG}|Fm\rangle \\ &= -(g_J - g_I)\mu_o H \left[ \frac{(F-I+J)(F-J+I)(I+J+F+1)(I+J-F+1)(F^2-m^2)}{4F^2(2F-1)(2F+1)} \right]^{1/2} \end{aligned} \tag{17}$$

For weak magnetic field the energy is given by the diagonal term and each hyperfine state splits linearly into 2F+1 substates. The equal spacing is disrupted in stronger fields as first the quadratic and then higher order terms become important.

For intermediate values of magnetic field, where $\mathcal{H}_{MAG}$ is of the same order as $\mathcal{H}_{HF}$, perturbation theory fails to give a convenient solution. In this case it is necessary to solve the secular determinant exactly. Since the interaction does not couple states differing in m, the total Hamiltonian matrix can be separated into 2F+1 sub-matrices, one for each value of m. The order of these sub-matrices is the number of F values which can have a projection m. For example, for $J = 1$, $I = 3/2$, there are two 1 x 1 matrices corresponding to $m = \pm 5/2$, $F = 5/2$; two 2 x 2 matrices corresponding to $m = \pm 3/2$, $F = 5/2, 3/2$; and two 3 x 3 matrices corresponding to $m = \pm 1/2$, $F = 5/2, 3/2, 1/2$. Thus the solution is reduced to diagonalizing each of these sub-matrices separately. It is feasible to do this with the aid of a digital computer.

Typical energy level diagrams for $J = 1$, $I = 3/2$ are shown in Figure 1. In the solution on the left, a small value of B was chosen; in the one on the right, a large value of B. In both cases, a negative value of A was used. Figure 2 shows solutions for $J = 2$, $I = 3/2$. It is worth noting that, since these diagrams show the dependence of energy on magnetic field, the slopes of the curves are related to the effective magnetic moments. In general, these are different in the different magnetic substates and change with magnetic field. However, in very strong fields where $\mathcal{H}_{MAG}$ is dominant, the moments approach the discrete values

$$\mu_{eff} \approx + g_J \mu_o m_J .$$

4. <u>Application to Atomic Beam Magnetic Resonance Experiments</u>

Atomic beam resonance experiments are carried out by observing transitions between the magnetic substates of an atom in a uniform field. These transitions, absorption and stimulated emission, are induced by

Figure 1

Zeeman energy levels for $J = 1$, $I = 3/2$ calculated for different values of hyperfine interactions. In the left-hand diagram the dipole interaction was assumed negative giving inverted level ordering. The right-hand diagram shows the level spacing for large quadrupole interaction and a small negative dipole interaction. The vertical arrows indicate the $\pi$ transitions observable in a flop-in atomic beam experiment.

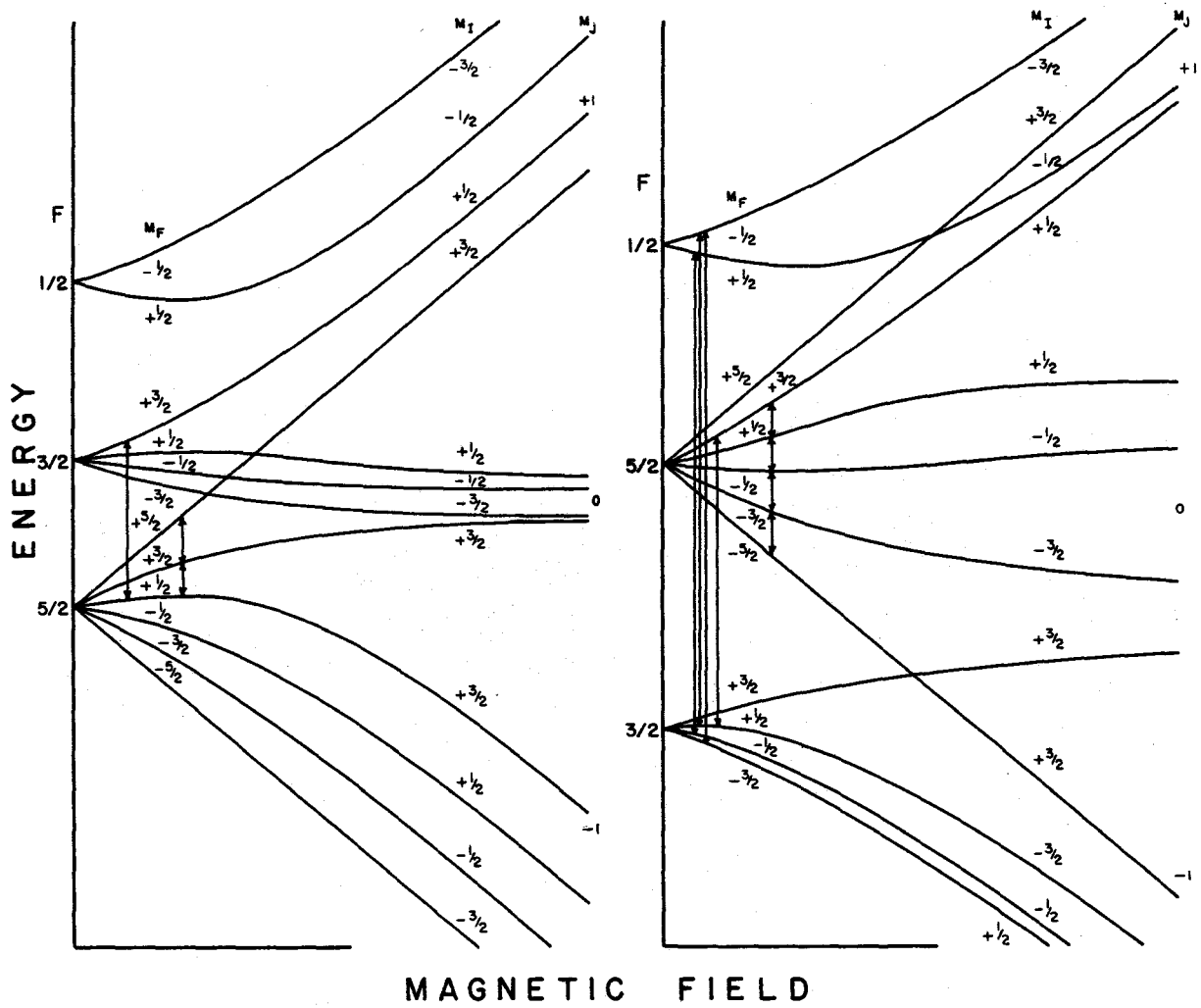
ENERGY
MAGNETIC FIELD
F
$M_F$
$M_I$
$M_J$
1/2
3/2
5/2
+1
0
-1

Figure 2

Zeeman energy levels for $J = 2$, $I = 3/2$ are shown for two different values of quadrupole interaction. The dipole interaction was assumed negative which causes the inverted level ordering apparent in the left-hand diagram. A large quadrupole interaction leads to the irregular level ordering observed in the right-hand diagram. The vertical arrows indicate the transitions observable in a flop-in atomic beam experiment.

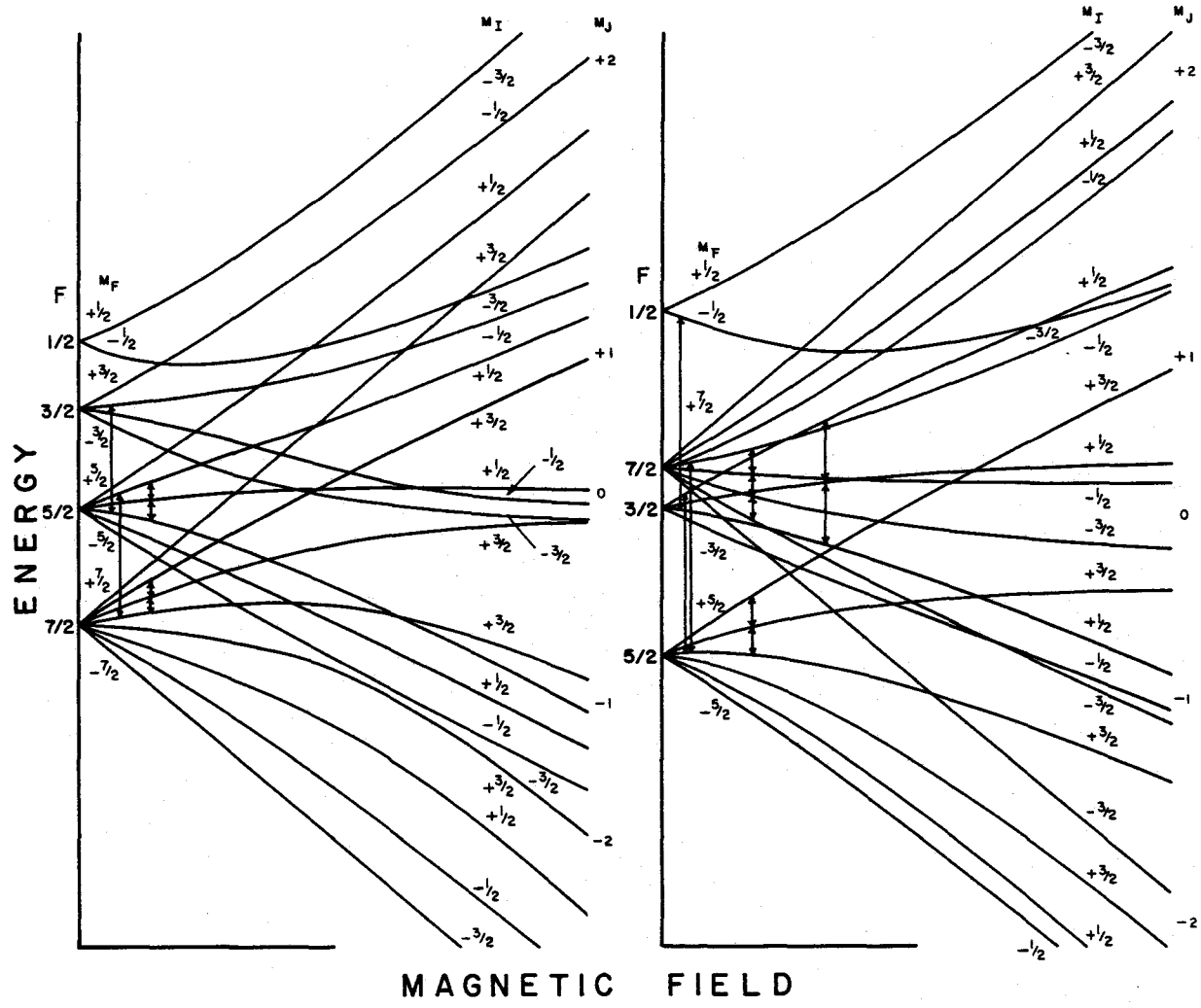
ENERGY
MAGNETIC FIELD
F
$M_F$
$M_I$
$M_J$
1/2
3/2
5/2
7/2
+2
+1
0
-1
-2

applying a radio-frequency oscillating magnetic field. The probability of spontaneous emission, of course, is negligible because of the low energy and magnetic dipole nature of the transitions.

The unperturbed transition frequency between states with energy $W_{Fm}$ and $W_{F'm'}$ is given by the Bohr condition

$$\nu_o = \frac{W_{Fm} - W_{F'm'}}{h} .$$

Although the natural width of the levels is very small due to their long lifetimes, the transition is actually observed over a range of frequencies. On the one hand, the perturbing r.f. magnetic field broadens the energy levels. In addition, since each atom experiences this perturbation for only a short time, $\delta t$, there is a further uncertainty

$$\delta \nu \approx \frac{1}{\delta t} \approx \frac{\overline{V}}{L}$$

where L is the length of the oscillating field region and $\overline{V}$ is the average velocity of the atoms. Weak r.f. fields may be treated as perturbations on the steady field and the transition probabilities can be calculated. Ramsey shows that this probability has a maximum for $\nu = \nu_o$ (Ramsey, 1956). Of course it vanishes unless the transition obeys the magnetic dipole selection rules:

| | | |
|---|---|---|
| $\Delta F = \pm 1$ | $\Delta m = 0$ | (for $\sigma$ transitions) |
| $\Delta F = 0, \pm 1$ | $\Delta m = \pm 1$ | (for $\pi$ transitions) |

The nomenclature is different from that used in optical spectroscopy because the transitions are magnetic rather than electric dipole (Kopfermann, 1958, pp 36).

Atoms can be made to undergo transitions in violation of the magnetic dipole selection rule by applying a stronger oscillating field.

Hack and others have calculated the probability of such multiple quantum transitions (Hack, 1956; Besset et al., 1954). The transition probability has a maximum for

$$\nu = \frac{1}{n}\left(\frac{W_{Fm} - W_{F'm'}}{h}\right) + \epsilon$$

where $\epsilon$ is a small correction dependent on the r.f. field strength and n is the number of quanta. If the oscillating field is not too strong $\epsilon$ can be neglected. The multiple quantum transitions of particular interest are $\pi$ transitions with the selection rules $\Delta F = 0$, $\Delta m = \pm n$.

Because of the condition imposed by the focussing magnets of an atomic beam apparatus, the only observable 'flop-in'* transitions are those between states which have equal and opposite effective magnetic moments in strong field. For atoms with half integral electronic angular momentum, all the above types of transition are observable and it is sufficient to use low r.f. power and examine only the single quantum transitions. However, for atoms with integral J (e.g. samarium), the only observable single quantum transitions are those with $\Delta F = \pm 1$. The $\Delta F = 0$ transitions which are most useful in the early stage of an investigation must necessarily involve multiple quanta.

a. Determination of Nuclear Spin

In a low magnetic field, where the energies of the Zeeman levels are given by only the first order term of the perturbation expansion (equations (16) and (17)), the splitting of adjacent levels of a hyperfine state $|IJF\rangle$ is

$$\nu = \frac{W_{Fm} - W_{Fm\pm1}}{h} = -\frac{\mu_0 H}{h}\left[g_J \frac{F(F+1)+J(J+1)-I(I+1)}{2F(F+1)} + g_I \frac{F(F+1)+I(I+1)-J(J+1)}{2F(F+1)}\right]$$

$$= -\frac{\mu_0 H}{h} \cdot g_F \qquad (18)$$

---

*Atomic beam machines are designated as 'flop-in' or 'flop-out' depending on whether the magnets are arranged to give an increase or a decrease in detected beam intensity at resonance.

Transitions between these levels satisfy the $\pi$ transition selection rules $\Delta F = 0$, $\Delta m = \pm n$ ($n = 1, 2 \ldots$). This expression forms the basis for the determination of the nuclear spin I. Usually J and $g_J$ are known for the element being studied, either from atomic spectra or atomic beam investigation, and the term in $g_I$ is small enough to be neglected in this approximation. For known H, J and $g_J$, then, the transition frequencies corresponding to different values of I (and $F = |\underline{I} + \underline{J}|$) can be calculated. It is a simple matter to see for which of these cases resonances are actually observed. In general, there may be resonances at the same frequency corresponding to different combinations of J and I, and caution must be exercised to prevent an erroneous assignment.

b. Determination of the Hyperfine Interaction Constants

Once a resonance has been observed and identified at low field, further experiments may be carried out in stronger magnetic fields to determine the hyperfine structure constants. In stronger magnetic field, the second order perturbation terms of equation (16) must be retained and these provide a correction to equation (18). This correction is proportional to $H^2$ and depends inversely on the separation of the hyperfine levels. Of course, it also depends explicitly on I, J and F and on $m_{INITIAL}$ and $m_{FINAL}$. The possible values of $m_I$ and $m_F$ can be determined by examining an energy level diagram such as Figure 1. This figure illustrates the fact that the number of quanta needed for an observable transition may depend on the values of the interaction constants. In the diagram on the left, the Zeeman transition requires 2 quanta but in the diagram on the right, 4 quanta are necessary. It is possible to obtain tentative values of the interaction constants from the field dependence of the transitions. Observations in still stronger magnetic fields will yield more accurate values of the constants. However, if $g_J \mu_o H/h$ is of the order of

$W_F - W_{F \pm 1}$, higher order perturbation theory will be required. In that event, it may be more convenient to use an exact solution of the secular determinant. A more direct way to measure the interaction constants would be to observe the hyperfine transitions at zero field. Their frequencies, $\nu = W_F - W_{F \pm 1}/h$ are strongly dependent on A, B and C (equation (13)). Thus a search for these transitions would be impractical without first having an accurate estimate of the frequencies involved. Such values could be obtained by the procedure outlined above.

It is not possible to actually use zero magnetic field since the atoms would then lose their magnetic quantization. Instead, the observations are made in weak magnetic field and the observed frequencies are corrected to their zero-field values using equation (16). Finally the set of linear equations derived from equation (13) can be inverted to yield A, B and C.

c. Other Determinations

The measurements of the preceding section permit precise determination of the hyperfine interaction constants and their relative sign. However, since only the separations of the hyperfine states are measured, the sign of any one of the constants is not determined. In particular, one cannot tell whether A, and therefore $g_I$, is positive or negative. There are several methods for determining this sign. The magnetic Hamiltonian (equation (15)) contains a term $g_I \mu_o m_I H$ previously neglected. The magnitude of $g_I$ can be determined from A by equation (14) and if this term is included in the secular determinant, solutions can be obtained assuming $g_I$ both positive and negative. If measured with sufficient precision, the experimental Zeeman frequencies will be consistent with only one choice of sign. Another method, less generally applicable, was used in these experiments and will be discussed in Chapter V with specific reference to the energy levels of samarium.

The nuclear gyromagnetic ratio can be determined from the interaction constant A. However, the calculation involves knowing $\langle 1/r^3 \rangle$ for the electrons. Unfortunately, there is a relatively large uncertainty in calculations of this kind due to our lack of knowledge of the atomic wave functions. Thus there is some advantage in precise experiments which permit a direct determination of $g_I$. These are necessarily performed at high field where the energy $g_I \mu_o m_I H$ is appreciable and the experiments rely on various schemes to eliminate the effect of the term in $g_J$ from the measurement (Pichanick et al., 1960; Cohen et al., 1962).

Although there are other methods of measuring the atomic gyromagnetic ratio $g_J$ (e.g. optical spectroscopy), none has the high precision obtainable by atomic beam measurement. In the case of atoms with I = 0, equation (18) simplifies, giving the exact relation

$$\nu = - \frac{\mu_o H}{h} g_J$$

Observations of these Zeeman transitions permit a precise direct measurement of $g_J$. The comparison of these experimental values with the theoretical values is an indication of the type of spin-orbit coupling.

# CHAPTER IV. ATOMIC BEAM APPARATUS AND EXPERIMENTAL TECHNIQUE

The atomic beam apparatus used in the present experiments has already been described in detail (King, 1960). Later modifications and its performance in hyperfine investigations were discussed elsewhere (Cameron, 1962; Cameron *et al.*, 1962). The description here will, therefore, be limited to the general features of the apparatus with specific reference to its use in the study of radioactive isotopes.

## 1. Principles of Operation

The material to be studied is evaporated from a source which is maintained at a temperature sufficient to produce a vapour pressure of between 0.1 and 1 millimeter of mercury. In Figure 3, a purely schematic diagram, this source is shown at O. The atoms stream into an evacuated chamber where the pressure is low enough to effectively eliminate gas scattering. Vertical slits define a narrow diverging beam of atoms which may reach the detector D. The beam passes, in succession, through two regions of strong magnetic field produced by what are called the A and B magnets. These magnets produce a strongly inhomogeneous field, whereas a third magnet, C, located between these two, produces a homogeneous field. In this region, there is also an oscillating field induced by a suitable antenna (not shown). This is usually a magnetic dipole loop driven by a variable frequency signal generator. An obstacle S, which may be withdrawn to permit alignment of the source, is positioned within the B magnet to block any straight-line paths from the source to the detector.

Figure 3

A plan view of an atomic beam apparatus showing idealized trajectories of atoms effusing from the source O. In a flop-in apparatus, with the fields and gradients of the A and B deflecting magnets as shown, atoms arrive at the detector D only if the sign of the atomic moment changes sign in the region of the uniform C field. The stop-wire S prevents undeflected atoms from reaching the detector. Collimating slits on the A and B magnets limit the beam.

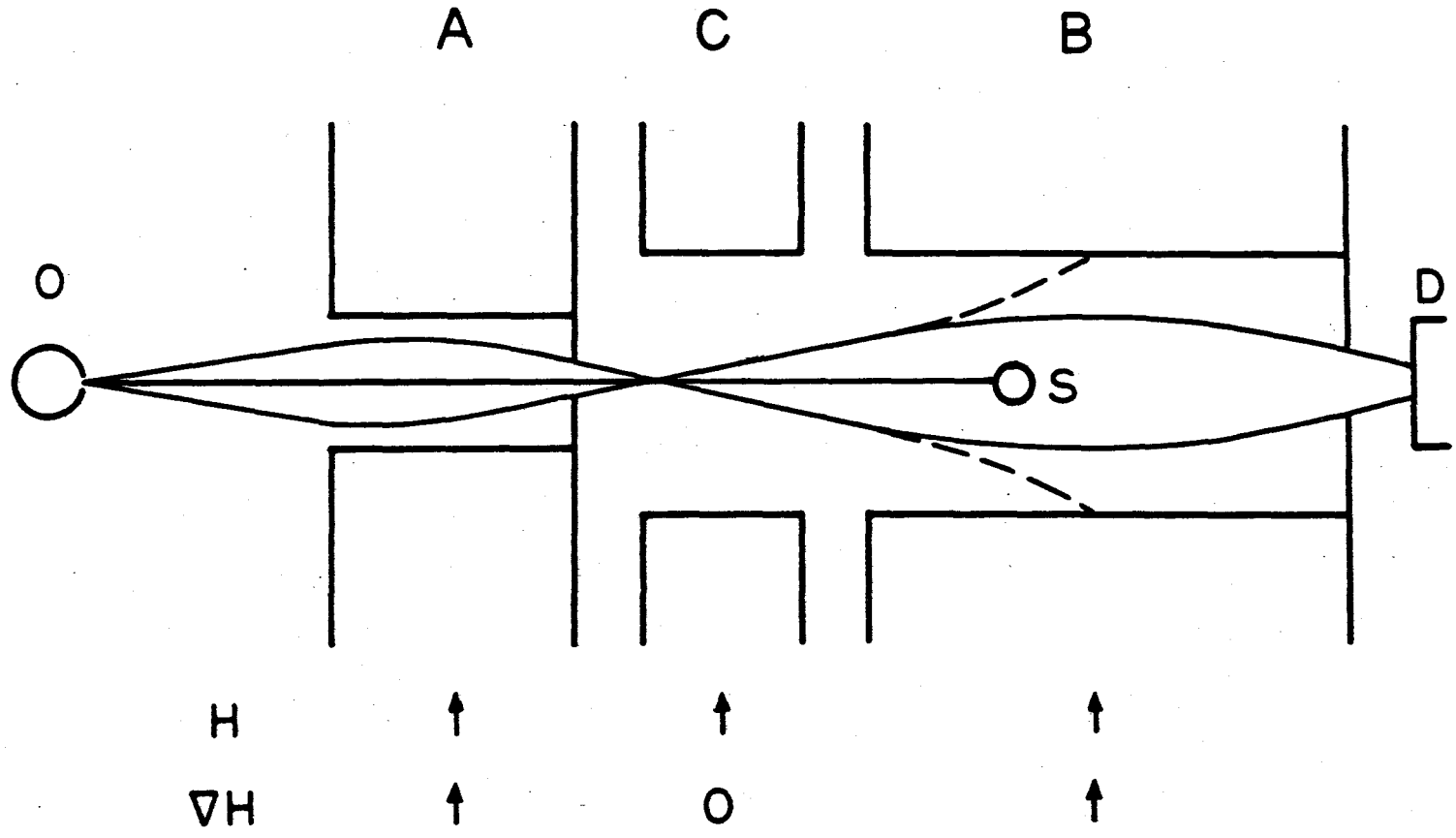
A
C
B
O
D
S
H
∇H
0

Because of its magnetic moment, an atom in a strong inhomogeneous field will be acted on by a force

$$\underline{F} = -\nabla W = -\frac{\partial W}{\partial H}\nabla H = +\mu_{eff}\,\nabla H \ .$$

The A and B magnets produce gradients parallel to the field and transverse to the beam axis as shown by the arrows. Thus the force, which is also transverse to the beam, causes the atoms to be deflected -- the amount of the deflection depending in each case on the effective magnetic moment and the length of time each atom spends in the field. As shown in Chapter III, for sufficiently strong magnetic field, $\mu_{eff} = +g_J\,\mu_o\,m_J$. In the atomic beam 'flop-in' configuration shown, the field gradients of the two deflecting magnets are in the same direction and, thus, any atoms which remain in the same substate during their passage from source to detector will suffer successive deflections in the same direction. These atoms will fail to pass through the exit slit as shown by the dotted trajectories in Figure 3. On the other hand, if an atom changes its magnetic substate in the C region so that $(m_J)_A = -(m_J)_B$, then the deflections cancel as shown by the solid trajectories. In fact, it is possible to choose the relative lengths of the magnets so that these 'flopped' atoms will return to the beam axis and pass through the detector slit for all velocities below a certain critical value. Above this velocity atoms will spend such a short time in the deflecting fields that their deflections will be too small to allow negotiation of the obstacle. Within this restriction, the machine has the property of velocity focussing.

The origin of the term 'flop-in' should now be clear. No atom will reach the detector unless it undergoes a transition which brings about a change in the sign of the high field quantum number $m_J$. For

such a transition to occur, the frequency of the oscillating field must correspond to the energy level spacing at that particular value of C field. In practice, some gas scattering does occur so that the condition of zero signal at the detector is not achieved. Nevertheless, when the resonance condition is satisfied, there will be a significant increase in the beam reaching the detector. The frequency of such a resonance is related, through the magnetic Hamiltonian in the previous Chapter, to the value of the C-field and the various electronic and nuclear parameters which characterize the atom.

2. Vacuum System

The main vacuum chamber consists of a welded aluminum box resting on a heavy duraluminum base plate. This box is removable to allow easy access to the magnet system which is arranged on the base plate. A similar but smaller box forms the oven chamber. Both are sealed separately to the base plate with neoprene gaskets. The two boxes are interconnected by a small buffer chamber whose walls are pierced by narrow openings to allow passage of the beam while restricting the flow of gas. Each chamber is pumped separately by one or more liquid nitrogen-trapped oil diffusion pumps. This system of differential pumping insures that the major portion of an atom's flight path is in the main chamber at a pressure of approximately $8 \times 10^{-7}$ mm Hg.

Two vacuum interlocks are used, each with two stages of pre-pumping -- one for inserting sources, the 'oven bar', and one for inserting collecting surfaces at the detector position, the 'button bar'. The latter facility is very important for sampling the beam arriving at the detector when using short half-lived material. Successive collecting surfaces must be inserted with a minimum of delay and without disturbing the high vacuum in the main chamber. In practice, a button can be removed and replaced by another in just over a minute.

3. Atom-Beam Source

The atom-beam sources are mounted on the oven bar which slides in through the oven chamber interlock. All the electrical leads for the sources pass through kovar seals in this bar so that the entire assembly can be removed from the vacuum. Two ovens are mounted, one for the element under investigation and one for the standard used in the calibration of the magnetic field.

Samarium metal was evaporated from a tantalum oven illustrated in Figure 4. An inner crucible of molybdenum was used to contain the sample and prevent creep. The adjustable slits were set .004" apart and the 1/8" -thick jaws channelled the effusing atoms in the forward direction. The screw-type lid was recessed to insure that it remained at the same temperature as the body of the oven. The original lid was found to run 50 to 100°C cooler due to radiation and poor thermal contact. The condensation of samarium on this surface caused a premature drop in the beam intensity. The oven was heated by electron bombardment from thoriated tungsten filaments suspended in front of the oven. By monitoring the accelerating voltage and emission current, it was possible to manually control the oven temperature to within a few degrees. The temperature was measured with a Leeds & Northrup (Model 8622-C) optical pyrometer.

The calibration oven is similar to that described above but, since it contained an alkali metal (usually sodium), a lower temperature was required. This oven was made of stainless steel and was directly heated with a tungsten heating element.

4. Magnet System

Figure 5, a perspective view of the atomic beam apparatus, shows the magnet system with the vacuum case removed. The end of the oven bar

Figure 4

An atomic beam source oven fabricated from a tantalum rod showing the adjustable slits and molybdenum crucible.

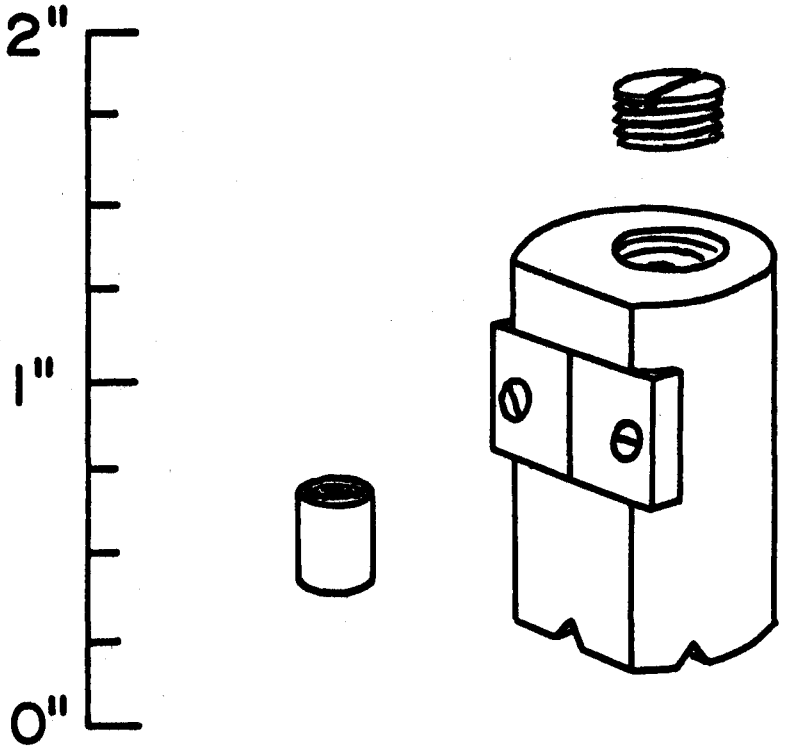
2"
1"
0"

Figure 5

A perspective view of the magnet system with the vacuum enclosure removed. The important features are numbered: (1) A-magnet, (2) C-magnet, (3) B-magnet, (4) Oven-bar interlock, (5) Detector bar interlock, (6) Stop wire mechanism. The insert at the lower left shows the cross-section of the A-magnet pole tips. The dashed rectangle indicates the region of field with uniform gradient.

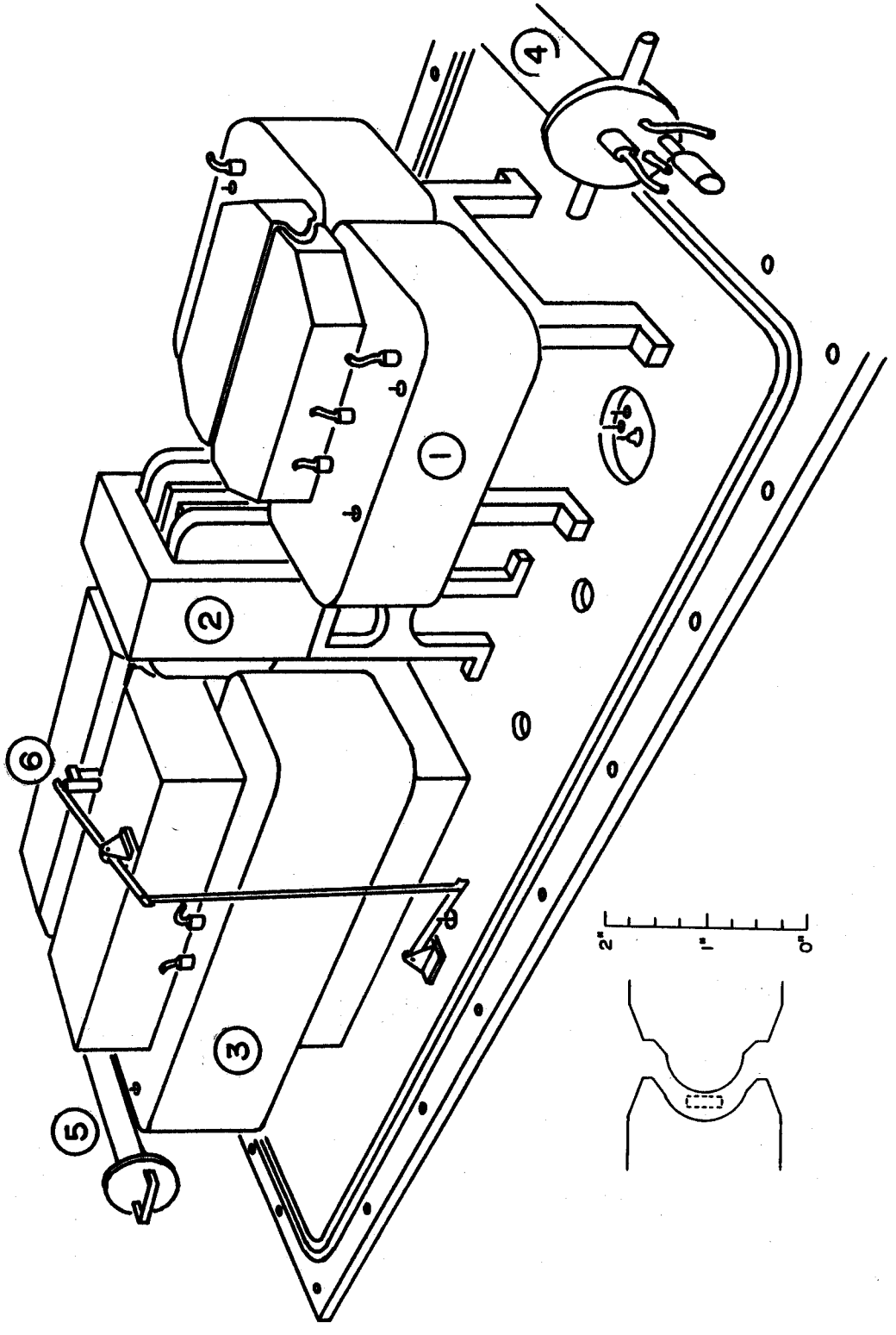
1
2
3
4
5
6
2"
1"
0"

can be seen at the right and the detector is on the left. The Armco iron pole tips of both deflecting magnets are sections of circular cylinders to provide a large region of approximately uniform field gradient. A cross-section of the A magnet pole tips is shown in the insert. The B magnet has similar shape with the linear dimensions increased by a factor of two to subtend approximately the same angle at the source.

The current for the high impedance windings of the A and B magnets is supplied by a current-regulated power supply capable of delivering up to 2 amperes at 2000 volts. These experiments were carried out using a current of 1 ampere which produces fields in the A and B magnets of 6.5 and 10 kilogauss respectively. This ratio, adjusted by shorting sections of the A magnet winding, was found to provide optimum focussing of samarium atoms.

The C magnet has plane parallel pole tips to provide a uniform magnetic field. Current for the windings of this magnet is supplied by a voltage stabilized power supply. Field drift due to a change of resistance of the windings was unimportant but that due to changes in the fringing field of the A and B magnets was bothersome. This was especially true for weak C field when the fringing produced the major contribution.

The C magnetic field was calibrated by observing the frequency of the Zeeman transition ($F = 2$, $m = -1 \Leftrightarrow F = 2$, $m = -2$) in a beam of sodium-23. This observed frequency was compared with a table of frequencies calculated at 0.1 gauss intervals using the known atomic and nuclear properties of this isotope. Between these calculated values a linear interpolation is accurate to $2 \times 10^{-4}$ gauss. In practice, the accuracy of the calibration is limited by the C field inhomogeneity which

broadens the sodium resonance to approximately 100 kc/sec (full width at half maximum). As a result, the peak position is uncertain to at least 2 kc/sec ($\sim 3 \times 10^{-3}$ gauss). Care must be taken to avoid over-powering the sodium resonance since multiple quantum transitions are then excited which, because of their different field dependence, distort the line shape.

5. Radio Frequency Equipment

The transitions observed in samarium range in frequency from 1 to 650 Mc/sec. Thus a variety of r.f. oscillators were required to provide the oscillating magnetic field. These oscillators are listed in Table I along with the manufacturers' specifications.

The r.f. loops used in these experiments are shown in Figure 6. Loop 'a' is a narrow U-shaped copper sheet terminating a section of coaxial line. This loop, oriented with its magnetic field parallel to the beam and perpendicular to the homogeneous C field, is used for exciting $\pi$ transitions ($\Delta m = \pm 1$). Loop 'b' is a section of vacuum-dielectric 50-ohm line terminated in a short circuit. The beam passes through slots in the side of the outer wall and close to the centre conductor. The magnetic field of this loop circulates about the centre conductor with components both parallel and perpendicular to the C field and so it is effective in inducing both $\sigma$ and $\pi$ transitions. Since the r.f. loops used do not constitute a matched impedance, care must be taken not to exceed the output-power rating of the generator. Several matching devices were used. A simple resistive T-attenuator was most convenient because of its broad-band characteristic and it transmitted sufficient power for inducing one- and two-quantum transitions.

The radio frequencies were monitored throughout the experiments using a Beckman model 7170 electronic counter and series 7570 frequency

TABLE I

Radio Frequency Oscillators

| Manufacturer | Model | Frequency Range Mc/sec | Power Output Watts |
|---|---|---|---|
| Tektronix | 190A | .35 - 50 | 2 into 50 ohms |
| General Radio | 1211C | .5 - 50 | .2 into 50 ohms |
| Wandel & Goltermann | LMS-68 | with the following plug-in units | |
| | LO-4 | 4 - 40 | 1 into 60 ohms |
| | LO-40 | 40 - 108 | 1 into 60 ohms |
| | LMS-681 | 75 - 160 | 1 into 60 ohms |
| | LO-170 | 170 - 330 | 1 into 60 ohms |
| | LO-325 | 325 - 610 | .5 into 60 ohms |
| | LO-610 | 610 - 960 | .5 into 60 ohms |

Figure 6

Two of the radio frequency loops used in the experiments: loop (a) for exciting $\pi$ transitions - a U-shaped dipole, loop (b) for exciting $\sigma$ transitions - a shorted coaxial line, slotted to permit passage of the beam.

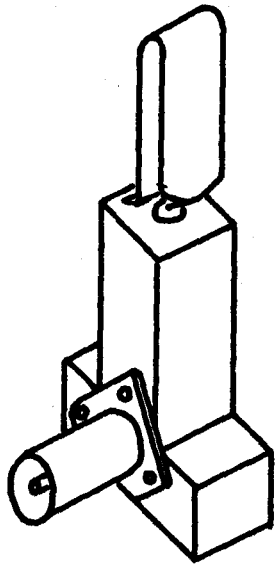

(a)

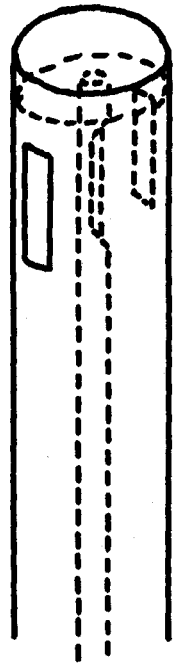

(b)

converters. The gating pulses for the counter and the reference frequencies for the converters are derived from the internal 1 Mc/sec crystal oscillator of the counter. This oscillator has a short-term stability of 1 part in $10^7$. Periodic checks against the 5 and 10 Mc/sec standard transmissions from WWV were made to correct for long-term drift. The overall accuracy of the frequency measurements is 1 part in $10^6$.

6. Beam Detection

The only practical method of detecting radioactive atoms of low isotopic abundance is to collect a number of atoms and observe their decay. Standardized collecting surfaces were exposed to the beam for a fixed interval of time using the button bar interlock. Subsequently, each surface was counted several times with a low background $\beta$ counter to determine the amount and half-life of the activity.

Each $\beta$ counter consists of a Philips (type 18515) end-window Geiger counter mounted inside a matching guard tube (type 18517). Eight such units are mounted in a frame supporting 2 inches of lead shielding and samples are positioned under the counting tubes with steel sliders. The pulses from each detector and associated guard tube are fed into a transistorized anticoincidence circuit and the net counting rate is observed with a scaler. With this arrangement the background counting rate is about 2 counts per minute.

The stable fraction of the samarium beam and the alkali metal calibrating beam were observed with a surface ionization detector. This method of detection, described in more detail by Ramsey, relies on the fact that a fraction of the atoms evaporating from a hot surface are emitted as ions (Ramsey, 1956). This is true if their ionization potential is lower, or at least not much larger, than the work function of the surface. A pure tungsten wire, two inches long and .010" in

diameter, was supported vertically to intercept the beam of atoms leaving the B magnet. This wire was heated to 1650°C by a current of 4.5 amperes and was maintained at a positive voltage to drive away the ions formed. The ion current was collected on a nichrome strip and measured by a Victoreen-Tullamore electrometer (model VTE-2). The background current from the wire, after flashing at 1800°C, was less than $10^{-13}$ amperes and very steady, whereas the detected beam current under operating conditions ranged from 1 to $5 \times 10^{-11}$ amperes.

7. Experimental Method and Analysis of Data

Preliminary to the experiment, the value of C field to be used and the range of frequencies to be scanned must be decided. For a spin search, this means choosing a value of field low enough so that Equation (18) is valid and large enough so that frequencies for different values of spin are separated by at least the experimental line width. For the later experiments, to determine the field dependance of the Zeeman transitions, it is desirable to set the field at as large a value as possible. However, if too strong a field is choosen there will be a large uncertainty in the predicted position of the resonance. This must not exceed the range of frequencies which can be scanned. This in turn is determined by the length of time the beam will last, the number of samples that may be counted and the degree of precision required. A search for the direct hyperfine transitions is possible when the uncertainty in their predicted frequencies is comparable to this range.

The C magnet field was adjusted and calibrated by observing the sodium resonance. The radioactive sample was inserted into the apparatus and heated to the temperature which would produce a steady beam lasting long enough to permit the required number of exposures. A series of buttons was then exposed at the predetermined frequencies. To correct for

fluctuations of the beam intensity, the ion current on the electrometer was noted before, and after, each exposure with the obstacle, or 'stop wire', removed. Also, every two or three resonance exposures was followed by a monitor exposure with the 'stop wire' out. These monitor exposures were used to correct for variation in the 'specific activity' of the beam.

The frequency of the calibration resonance is checked once or twice during the experiment as well as at the end in order to keep track of any field drift.

A computer program was used to fit the counting data from each button with a compound exponential curve. The number of exponentials and their decay constants were chosen to correspond to the activities observed in a sample of the source material, but the amount of each activity was treated as a parameter in the least squares fit. The initial activity of the isotope being studied was corrected for fluctuations in beam intensity and for counter efficiency. The values so obtained and their statistical uncertainties were plotted against their corresponding r.f. frequencies to yield a resonance curve.

## CHAPTER V. THE SAMARIUM EXPERIMENTS AND THEIR RESULTS

The preceding chapters have dealt with the theory and equipment used in atomic beam experiments. Since the variety of practical problems encountered in these experiments are closely related to the nuclear, atomic and physical properties of samarium these will be discussed in the first part of this chapter. The experimental results follow in the second part.

The arc and absorption spectra of rare earth mixtures were investigated by King and Paul respectively (King, 1935; Paul, 1936). An analysis of these data was made by Albertson. On the basis of the septet multiplet in the neutral spectrum of samarium, he deduced that the eight electrons outside the xenon core have the configuration $4f^6\ 6s^2$ and these must couple to give the Hund's rule term $^7F$ (Albertson, 1935). Since the f shell is less than half filled, the state $J = 0$ has lowest energy. The experimental fine structure in Figure 7 shows a moderate deviation from the Landé interval rule for L-S coupling. The $g_J$ values calculated in the L-S limit are all (with the exception of the state $J = 0$, of course) the same, 1.501156 (10); the experimental values are listed in Table II. These were measured for the even-even samarium isotopes by atomic beam magnetic resonance (Woodgate, 1961).

Recently the rare earth elements have become available as pure metals and these have been the subject of many physical and chemical investigations. One of these was the measurement of the heat of

Figure 7

The fine structure of the ground multiplet of the samarium atom showing the population of each state at 1220°K. For a nuclear spin I = 3/2 each fine structure state is split into hyperfine states. This is shown schematically for the lowest multiplet levels.

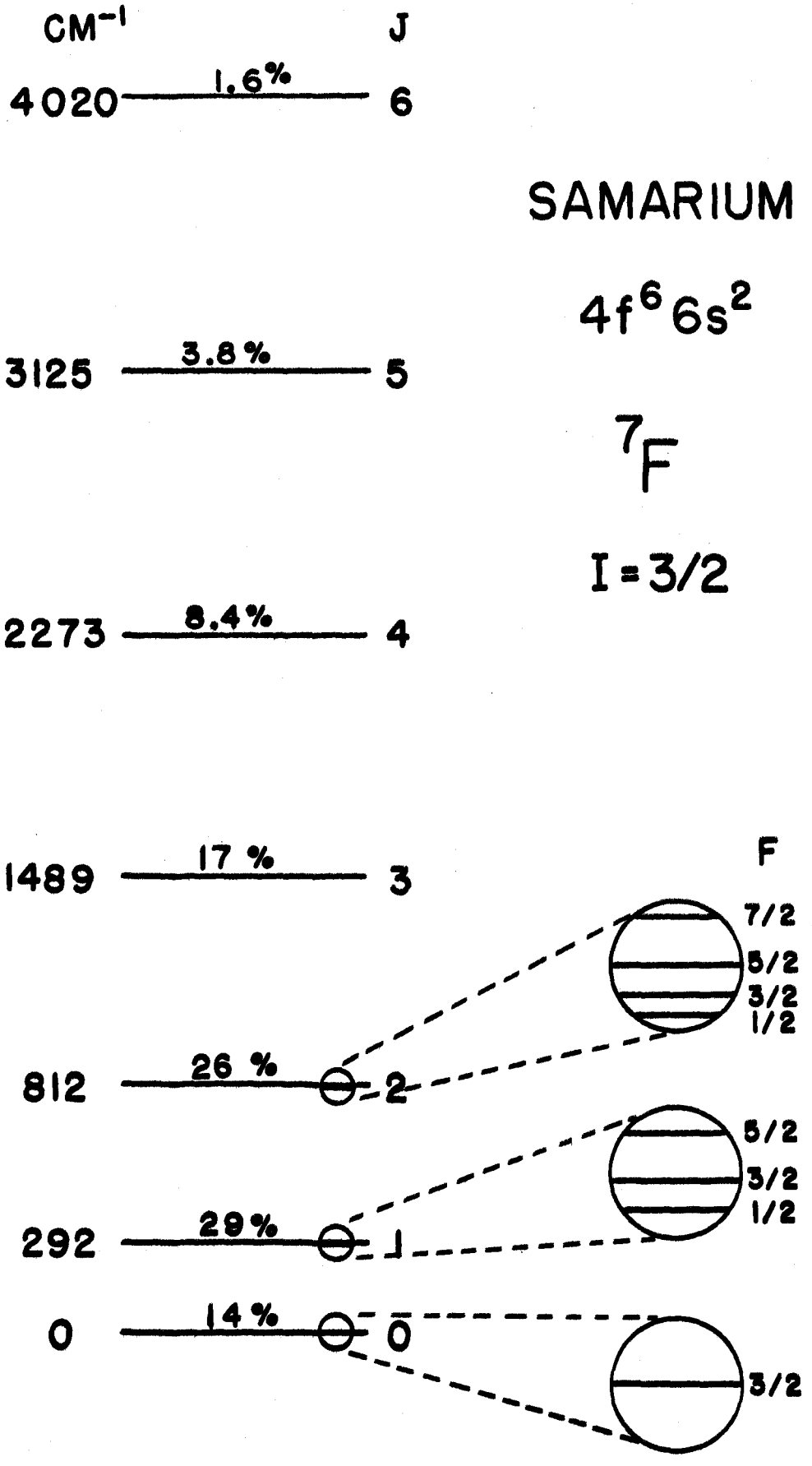
CM⁻¹
J
4020
1.6%
6
SAMARIUM
4f⁶6s²
3125
3.8%
5
⁷F
I = 3/2
2273
8.4%
4
1489
17 %
3
F
7/2
5/2
3/2
1/2
812
26 %
2
5/2
3/2
1/2
292
29%
1
0
14%
0
3/2

TABLE II

Samarium Fine Structure

| J | $g_J$ | Population of Fine Structure States at 1220°K | Population per Magnetic Substate I = 3/2 | Relative Resonance Intensity |
|---|---|---|---|---|
| 0 | | 13.8% | 3.45% | |
| 1 | 1.49840(5) | 29.3% | 2.44% | 100 |
| 2 | 1.49779(3) | 26.5% | 1.32% | 54 |
| 3 | 1.49707(3) | 16.6% | 0.60% | 24 |
| 4 | 1.49625(4) | 8.4% | 0.23 | 10 |
| 5 | 1.49533(6) | 3.8% | 0.08 | 3.3 |
| 6 | 1.49419(10) | 1.6% | 0.03 | 1.3 |

sublimation of samarium (Savage et al., 1959). From this one can estimate that the vapour pressure at 1300°K is about 0.4 mm Hg, well within the range mentioned in Chapter IV suitable for producing a beam. One reference lists the vapour pressure of samarium as ten times higher than this (Beavis, 1960). In our experiments, samarium beams were observed and the intensity varied logarithmically over the range 1200°K to 1500°K. For temperatures below this, the beam was not detectable and above this range the source pressure is high enough that the atoms do not effuse individually but form a jet of gas.

Because of the low fine structure energy, all the states of the ground multiplet are populated at the source temperature. The population can be calculated from the Boltzmann distribution function

$$\frac{N_J}{N_o} = (2J + 1)\, e^{-W_{oJ}/kT}$$

where $W_{oJ}$ is the energy of the fine structure state $^7F_J$. The relative population at a beam temperature of 1220°K is shown in Figure 7. Of course, if the nucleus has a spin $I \neq 0$, each of these states is split by the hyperfine interaction. Since this splitting is small, the population of each fine structure state is divided equally among its hyperfine states. The intensity of an atomic beam resonance is inversely proportional to the total multiplicity of the fine structure state because only two of these $(2J + 1)(2I + 1)$ sub-states contribute to any one resonance. Table II shows the calculated relative intensities of resonances in each fine structure state for $I = 3/2$. Atoms in the state $J = 0$ have no electronic magnetic moment and they, along with the fraction of atoms with $m_J = 0$ in states with non-zero J, are undeflected.

Furthermore, the atoms in the high velocity tail of the Boltzmann distribution spend such a short time in the deflecting fields that they are essentially undeflected. A measure of the effectiveness of the deflecting magnets is the decrease in detected beam intensity when they are turned on. For samarium this is about 60%, an indication that nearly all of the undeflected atoms are those with zero moment. When the stop wire is inserted it must prevent the undeflected portion of the beam from reaching the detector in order to ensure a good signal-to-background ratio on resonance exposures.

The radioactive samarium isotopes were produced by irradiation of samarium metal in the thermal neutron flux of the McMaster reactor. The samples to be irradiated were sealed in quartz vials and consisted of 50 to 100 mg of 99.9% pure samarium metal turnings. The natural isotopic constitution of samarium is shown in Table III; also listed are the neutron capture cross-sections, the reaction products and their half-lives. For short irradiations the only significant activities produced are due to $Sm^{153}$ and $Sm^{155}$. Preliminary samples were irradiated and the $\gamma$-ray spectra observed with a NaI(Tl) scintillation spectrometer and multichannel analyser. The only components observed were consistent with the decay of these two isotopes. The $\beta$ counters described previously were eminently suitable for counting samples of these isotopes because of the high energy $\beta$ groups in their decay. Effects due to the two isotopes could be resolved because of the large difference in their half-lives.

The long half-life, low decay energy and presumably small production cross-section of $Sm^{151}$ precludes it being observed. If experiments are to be carried out with this isotope the source will have

TABLE III

Samarium Isotopes

| Mass | Abundance (Percent) | Thermal Neutron Capture Cross-Section x $10^{-24}cm^2$ | Reaction Product | Half-Life |
|---|---|---|---|---|
| 144 | 3.09 | 0.03 | $Sm^{145}$ | 340 days |
| 147 | 14.97 | | $Sm^{148}$ | Stable |
| 148 | 11.24 | | $Sm^{149}$ | Stable |
| 149 | 13.83 | 41,500 | $Sm^{150}$ | Stable |
| 150 | 7.40 | | $Sm^{151}$ | 80 years |
| 152 | 26.72 | 135 | $Sm^{153}$ | 47.1 hours |
| 154 | 22.71 | 5.3 | $Sm^{155}$ | 23.5 minutes |

to be obtained, by a different method, as a fission product, or after an extended irradiation in a high flux reactor. One approach which was considered was the irradiation of neodymium to produce $Sm^{151}$ by the reaction

$$Nd^{150} + n \rightarrow Nd^{151} \xrightarrow{\beta \text{ decay}} Pm^{151} \xrightarrow{\beta \text{ decay}} Sm^{151}$$

The $Sm^{151}$ could then be separated chemically.

The large neutron capture cross-section of $Sm^{149}$ causes self-shielding of the sample. Although adequate $Sm^{153}$ activity was obtained, the $Sm^{155}$ experiment would have been considerably easier with isotopically-enriched $Sm^{154}$. This would give higher effective flux, higher specific activity of $Sm^{155}$ and lower $Sm^{153}$ background.

The McMaster reactor has two types of irradiation position. In one case, the sample is sealed in an aluminum can and irradiated in an aluminum sample holder within the core assembly. In this location the neutron flux is approximately $1.5 \times 10^{13}$ n/cm$^2$/sec. However, the radiation hazard due to the activity induced in the can and sample holder restricts the rapid delivery of the samples. This was not a handicap in the $Sm^{153}$ experiments since the samples were left for several hours, in any case, to let the $Sm^{155}$ activity decay. After irradiation, the samples were brought to the hot laboratory, adjacent to the atomic beam apparatus, in a lead 'castle'. The aluminum can was opened and the quartz capsule removed with tongs and transferred to a sealed dry box. Here the elongated tip of the capsule was broken and the samarium poured into a waiting tantalum oven. The oven was then inserted into the apparatus, using the over-bar interlock, and heated to beam temperature.

For the $Sm^{155}$ experiments, because of its short half-life (23.5 minutes), it was necessary to obtain the samples as soon as possible after

irradiation. In this case the pneumatic 'rabbit' facility was used. The samples to be irradiated were placed in polyethylene containers which were dispatched by compressed air to a position in the pneumatic tube parallel to the reactor core face. The flux at this position was not calibrated but a comparison of samples irradiated at the two locations indicated a flux of approximately $5 \times 10^{12}$ n/cm$^2$/sec. Seconds after the end of a one-hour irradiation, the 'rabbit' was received in the hot laboratory. The time saved in delivery compensates for the lower flux, yielding a sample with a higher ratio of $Sm^{155}$ to $Sm^{153}$ activity. The sample was then handled by the procedure outlined above; with practice a beam could be obtained within ten minutes from the end of the irradiation.

Detection of the radioactive samarium requires that a sample of the beam be collected on a surface for counting. A preliminary experiment was carried out to test the relative sticking efficiency of samarium atoms on several different collecting surfaces. Three of the surfaces, freshly plated copper and silver, and flamed platinum, had the same efficiency within about 20%. Antimony, carbon and sulphur surfaces were considerably less efficient. Since the material and technique for making reproducible copper surfaces was at hand (King, 1960; Cameron, 1962), these were used for the remainder of the experiments. To prevent accidental loss of the activity and possible contamination of the counters, each exposed 'button' was sprayed with a thin coat of plastic lacquer immediately after removal from the atomic beam machine.

The stable samarium beam was detected by surface ionization on a tungsten wire heated to 1650°C. Although no deliberate steps were

taken to oxidize the wire, it was observed that the detector's sensitivity varied almost linearly with the main chamber pressure in the range from 5 to 20 x $10^{-7}$ mm of Hg. Ramsey has pointed out that oxidized tungsten has a higher work function than pure tungsten and so has a higher ionization efficiency (Ramsey, 1956). Presumably the partial pressure of oxygen in the 'vacuum' was still sufficient to form an oxide layer on the hot tungsten.

1. The Samarium-155 Experiment

The short half-life of $Sm^{155}$ made it imperative to conduct the experiment as rapidly as possible. With this in mind, the oven was heated to a temperature of 1100°C which permitted a 100-mg sample to be evaporated in only forty minutes. This is sufficient time to expose six resonance buttons for $2^1/2$ minutes each and three monitor buttons for $^1/2$ minutes each, allowing one minute for each button change and a few minutes' safety margin. With the exception of the first and last monitor buttons, which were alternated in one of the β counters, each button was counted continuously. The decay of each sample was followed closely for the first two hours and then longer counts were taken to find the amount of 47-hour $Sm^{153}$ activity. The counting rates were fitted to two exponentials by least squares. The decay of a typical resonance exposure is shown in Figure 8.

Using equation (18) and the known $g_J$ values of samarium, the frequencies of the Zeeman multiple quantum transitions were calculated. A spin search was conducted at low field for the J = 1 resonance which should have the highest intensity because of the low multiplicity and high population of this state (Table II). Exposures were made at the frequency corresponding to $\Delta m = \pm n$ in the state F = I + J for

Figure 8

Decay of a $Sm^{155}$ resonance exposure. The experimental curve is broken into 23.5-minute and 47-hour components.

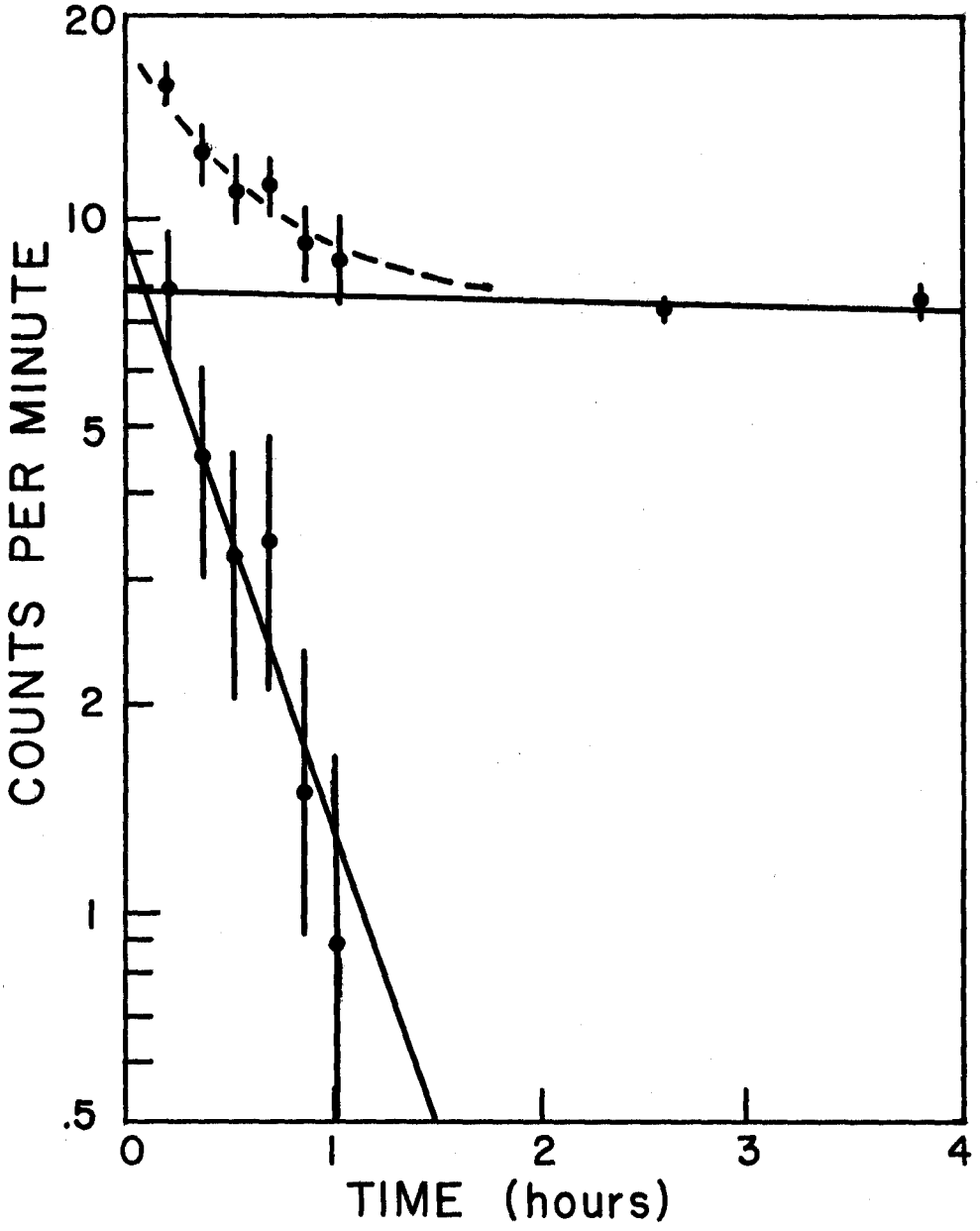
20
10
5
2
1
.5
COUNTS PER MINUTE
0
1
2
3
4
TIME (hours)

$J = 1$, $I = 1/2$, $3/2$, $5/2$, $7/2$, $9/2$ and $11/2$ and for $J = 2$, $I = 3/2$. As a further check the $F = 5/2$, $J = 2$, $I = 3/2$ resonance was confirmed. Table IV shows the frequencies and fields for which resonances were observed, the state to which they are assigned and, for comparison, the observed and calculated $g_F$ values. The $J = 2$, $I = 3/2$ resonances in a field of 2.54 gauss are shown in Figure 9.

The accumulated results of the eight runs are shown in the upper portion of Figure 10; the lower portion of this figure shows the calculated frequencies for $J = 1$, 2 and 3 resonances. The abscissa is the normalized frequency $\frac{h\nu}{\mu_0 H}$ which, at these low fields, is just $|g_F|$ (equation (18)). In the upper portion the ordinate is the normalized 23.5-minute activity, and in the lower, it is the possible half integral values of spin. Although for any one resonance there is some ambiguity as to which value of spin it corresponds, the composite spectrum is only consistent with $I = 3/2$.

In view of the difficulty of these experiments -- short half-life, low activity and the $Sm^{153}$ background -- it was deemed impractical to proceed with the further study of the hyperfine structure of $Sm^{155}$. After a complete study of $Sm^{153}$, which has the same spin and which might be expected to have similar hyperfine splittings, the $Sm^{155}$ investigation would be more feasible.

2. <u>The Samarium-153 Experiments</u>

Because of the long half-life of $Sm^{153}$ (47 hours), these experiments could be conducted at a more leisurely pace. Longer irradiations of ten to twenty hours made it possible to obtain samples with high specific activity (about 1 mC/mg). The samarium was evaporated at a lower temperature of 950°C so that a 100-mg source

TABLE IV

Samarium-155 Results

| Transition | H gauss | $\nu$ Observed Mc/sec | $h\nu/H\mu_o = g_F$ | $g_F$ calculated |
|---|---|---|---|---|
| J = 1, F = 5/2 | 1.945(7) | 1.675(50) | 0.615(25) | 0.600 |
| | 2.375(15) | 2.030(50) | 0.610(15) | |
| | 3.700(7) | 3.140(50) | 0.605(12) | |
| J = 2, F = 7/2 | 2.525(7) | 3.075(30) | 0.872(10) | 0.855 |
| | 3.700(7) | 4.450(50) | 0.858(10) | |
| | 4.560(7) | 5.510(50) | 0.864(10) | |
| J = 2, F = 5/2 | 2.540(7) | 3.400(30) | 0.956(10) | 0.940 |

Figure 9

Two resonances observed in $Sm^{155}$ experiments. These were attributed to $J = 2$, $F = 7/2$ and $5/2$ Zeeman transitions for $I = 3/2$.

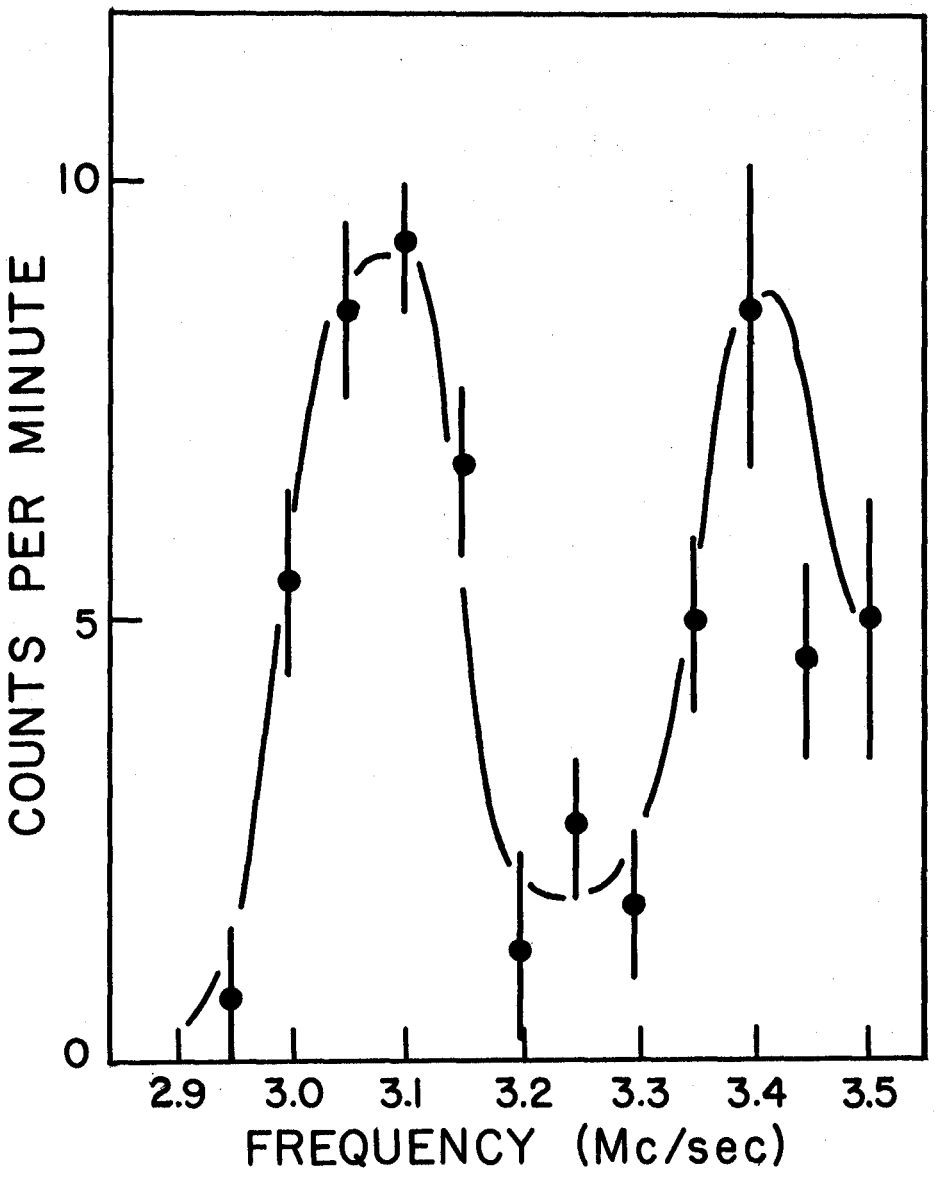
10
5
0
COUNTS PER MINUTE
2.9
3.0
3.1
3.2
3.3
3.4
3.5
FREQUENCY (Mc/sec)

Figure 10

The composite results of the $Sm^{155}$ experiments are plotted in the upper portion of this diagram. The circles represent points observed in spin searches. The solid curve outlines the resonances observed. Calculated Zeeman spectra are indicated below for the half integral values of spin for J = 1, 2 and 3.

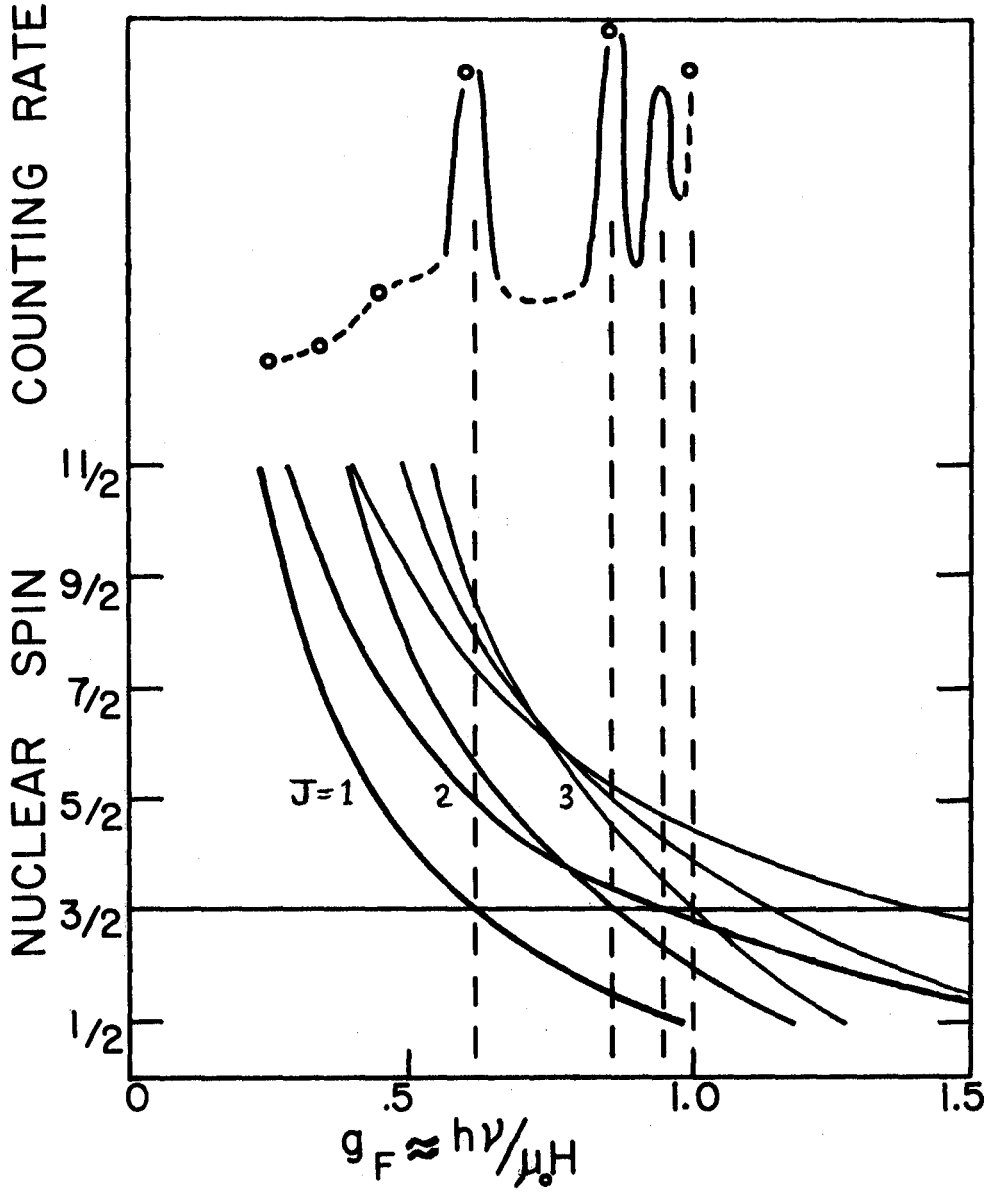
COUNTING RATE
NUCLEAR SPIN
11/2
9/2
7/2
5/2
3/2
1/2
J=1
2
3
0
.5
1.0
1.5
$g_F \approx h\nu/\mu_0 H$

produced a steady beam lasting five to seven hours. In this time as many as fifty resonance exposures were obtained from a single source. These samples were divided among seven of the β counters and counted in rotation until adequate counting statistics had been accumulated or the samples had decayed. The remaining counter was used for the monitor exposures which, along with the hot wire detector current, were used for beam normalization.

a. The Zeeman Transitions

The nuclear spin of samarium-153 had been reported previously as 3/2 (Cabezas et al., 1959). It was then a simple matter to use equation (18) to calculate the nominal frequencies of all the possible Zeeman transitions at low field. These are shown in Figure 11 for $J = 1, 2, 3$, and 4. The solid lines are the transitions observable for normal hyperfine level ordering and the broken lines indicate the positions of additional transitions which are only observable for special cases of hyperfine ordering. The height of each line represents the calculated relative intensity of the corresponding two quantum resonances, taking into account the population and multiplicity of each fine structure state.

The first experimental step was to observe several of these at low field to identify the resonances, establish their actual intensity and check our techniques of observing double quantum transitions. The spectrum observed at 3.68 gauss is shown in Figure 12. Although some of the resonances could be identified unambiguously, several peaks were broadened and distorted. For instance, a bump was observed, on several occasions, on the high frequency side of the $J = 2$, $F = 5/2$ peak.

Figure 11

Calculated spectrum of Zeeman transitions in samarium ($I = 3/2$). The broken lines represent transitions which may be observed in a 'flop-in' apparatus only for special cases of hyperfine level ordering. The heights of the lines are proportional to the expected resonance intensities.

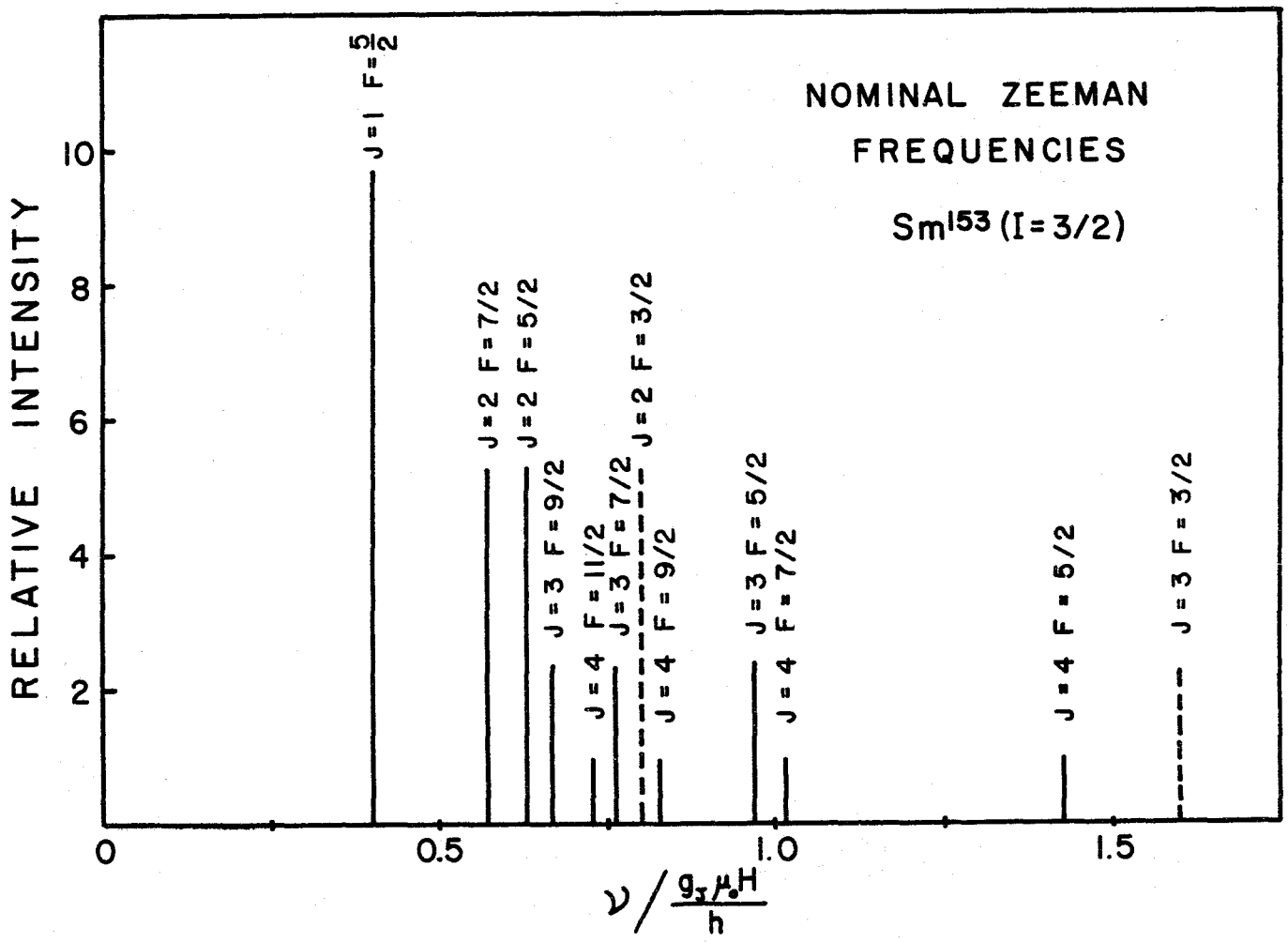
NOMINAL ZEEMAN
FREQUENCIES
Sm153 (I = 3/2)
RELATIVE INTENSITY
10
8
6
4
2
0
0.5
1.0
1.5
ν / gJμ₀H / h
J = 1 F = 5/2
J = 2 F = 7/2
J = 2 F = 5/2
J = 3 F = 9/2
J = 4 F = 11/2
J = 3 F = 7/2
J = 2 F = 3/2
J = 4 F = 9/2
J = 3 F = 5/2
J = 4 F = 7/2
J = 4 F = 5/2
J = 3 F = 3/2

Figure 12

Spectrum of Zeeman transitions observed in $Sm^{153}$ at 3.68 gauss. The solid lines indicate the nominal and calculated positions of resonances and the number indicates the number of quanta necessary to produce the resonance. The calculated positions are for $A_2 = -2.6$ Mc/sec and $B_2 = 306$ Mc/sec.

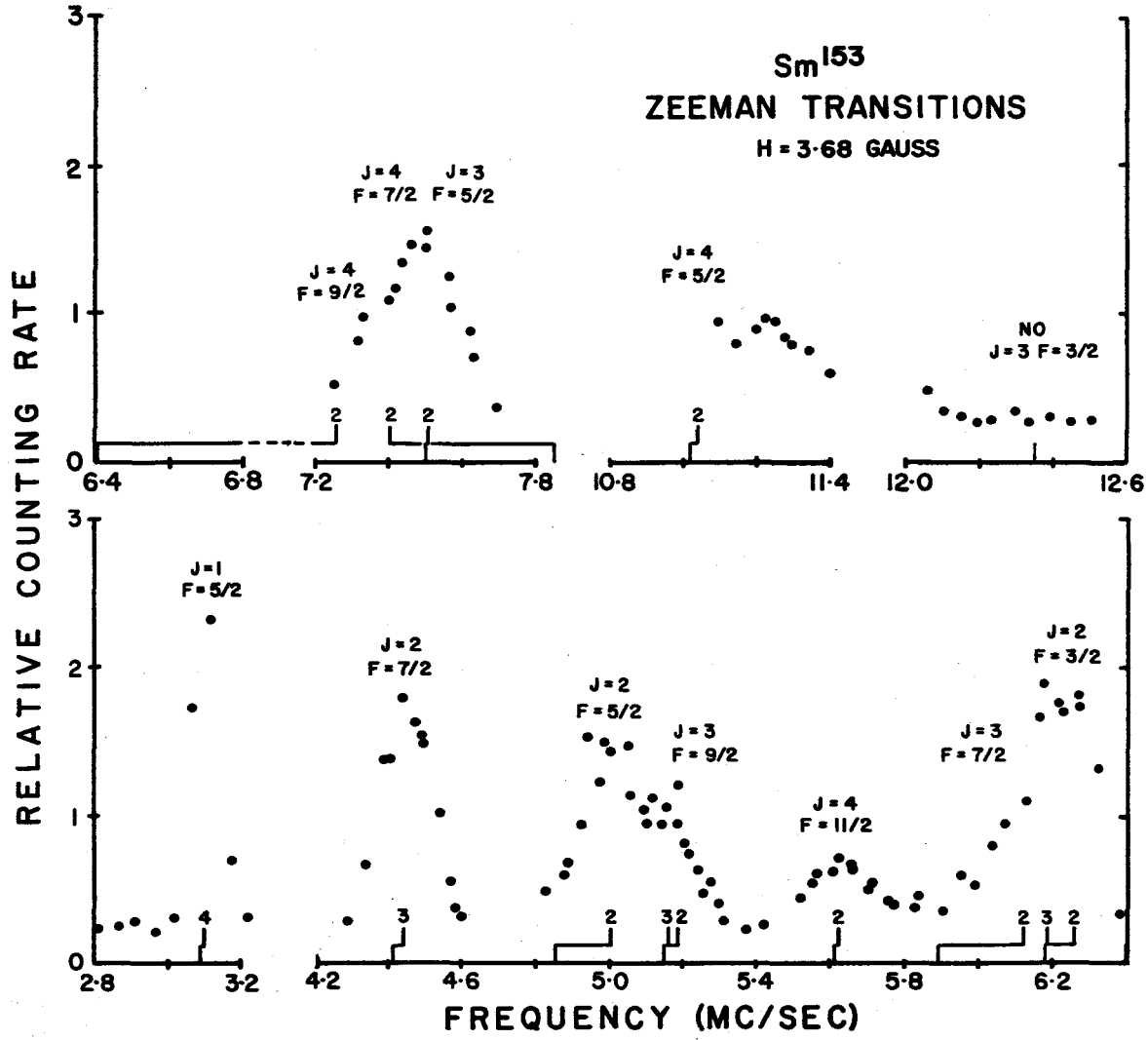
Sm153
ZEEMAN TRANSITIONS
H = 3·68 GAUSS
J = 4 F = 9/2
J = 4 F = 7/2
J = 3 F = 5/2
J = 4 F = 5/2
NO J = 3 F = 3/2
J = 1 F = 5/2
J = 2 F = 7/2
J = 2 F = 5/2
J = 3 F = 9/2
J = 4 F = 11/2
J = 3 F = 7/2
J = 2 F = 3/2
RELATIVE COUNTING RATE
FREQUENCY (MC/SEC)

This was attributed to the $J = 3$, $F = 9/2$ resonance. No attempt was made to observe transitions in the $J = 5$ and $J = 6$ fine structure states. From Table II their intensity would be less than one-third that of the $J = 4$ resonances.

From these low field data three significant observations can be made immediately. Firstly, the peak in the vicinity of 6.2 Mc/sec is too large to be just the $J = 3$, $F = 7/2$ resonance; also, it appears to be double. The only other resonance which could contribute here is that due to $J = 2$, $F = 3/2$. There is an observable transition in this hyperfine state only if it lies between the $F = 5/2$ and the $F = 7/2$ levels. In general, this is the case for $B_2/A_2 > 4$ or $< -24$. (Figure 2 showed an example of this particular ordering.) Secondly, there is no resonance at the frequency predicted for $J = 3$, $F = 3/2$. This is the case if $B_3/A_3$ is greater than 30 or less than 3.33. Of course, one cannot exclude the unlikely possibility that the resonance would have been found if the search range had been extended. Finally, the $J = 1$, $F = 5/2$ resonance is less intense and narrower than the $J = 2$ resonances. This could be anticipated if it were a four quantum resonance as shown in Figure 1, a condition that prevails for $B_1/A_1 < -2$ or $> 4$. These conclusions were, in fact, confirmed by later experiments.

It might have been possible to follow each resonance to higher field and thus determine the interaction constants for each state independently. However, even neglecting the octopole interaction, there were eight constants to be determined and an alternative approach was desirable. The nuclear contributions to equations (14) are independent of the electronic state and so can be factored. Thus it is possible to express the constants for each state in terms of those for the $J = 2$

state only. The ratios $A_J/A_2$ and $B_J/B_2$ are shown in Table V. Woodgate has recently measured the hyperfine constants for $Sm^{147}$ and $Sm^{149}$ and their ratios are shown also (Woodgate, 1963). The experimental ratios were used because they do not involve the assumption that the coupling in samarium is pure Russell-Saunders. The preceding limits then restrict the ratio $B_2/A_2$ to three regions, namely, less than -24, between 4 and 7.45, or greater than 67.7. In all three regions, the $J = 1$, $F = 3/2$ resonance requires four quanta. In the small range $4 < B_2/A_2 < 7.45$, the $J = 2$, $F = 7/2$ resonance would be a two quantum transition. In the other two regions it requires three quanta. Since these resonances are well separated from the rest, it was originally planned to observe them at higher field to find their quadratic shifts. Unfortunately, the probability of the higher order transitions drops off rapidly as the field is increased, as shown in Figure 13, and this approach had to be abandoned. This effect is understandable because, as the field increases, the spacing of the levels becomes more and more unequal and the r.f. frequency, which is optimum for one part of the transitions, cannot excite the other. This will be more serious in transitions involving four or five states than in a transition involving only three.

None of the two quantum resonances was clearly resolved at low field. However, it was hoped that they would be in a higher field. Accordingly, some of these transitions were observed in fields of 5 and 7 gauss. Although the resonances were still not resolved, small shifts were apparent which, to second order perturbation theory, were consistent with $B_2/A_2$ approximately -45 and $|A_2|$ approximately 4 Mc/sec. These values were not very accurate. However, they did serve to indicate that the field would have to be increased in small steps in order to avoid

TABLE V

Ratios of Hyperfine Constants

| | Calculated Ratios for L-S Coupling | Experimental Ratios (After Woodgate) | |
|---|---|---|---|
| | | $Sm^{147}$ | $Sm^{149}$ |
| $A_1/A_2$ | 0.93750 | 0.81342(5) | 0.81332(3) |
| $A_3/A_2$ | 1.09375 | 1.219841(8) | 1.219898(8) |
| $A_4/A_2$ | 1.21875 | 1.44977(24) | 1.44966(8) |
| $B_1/B_2$ | 0.95455 | 0.94334(16) | 0.94256(28) |
| $B_3/B_2$ | 0.53030 | 0.541398(85) | 0.54090(30) |
| $B_4/B_2$ | -0.34711 | (-)0.33946(276) | (-)0.33957(610) |

Figure 13

The rapid decrease in intensity of the $J = 1$, $F = 5/2$ resonance as the magnetic field is increased is shown by these resonances. The beam intensity and r.f. power were approximately the same in each case.

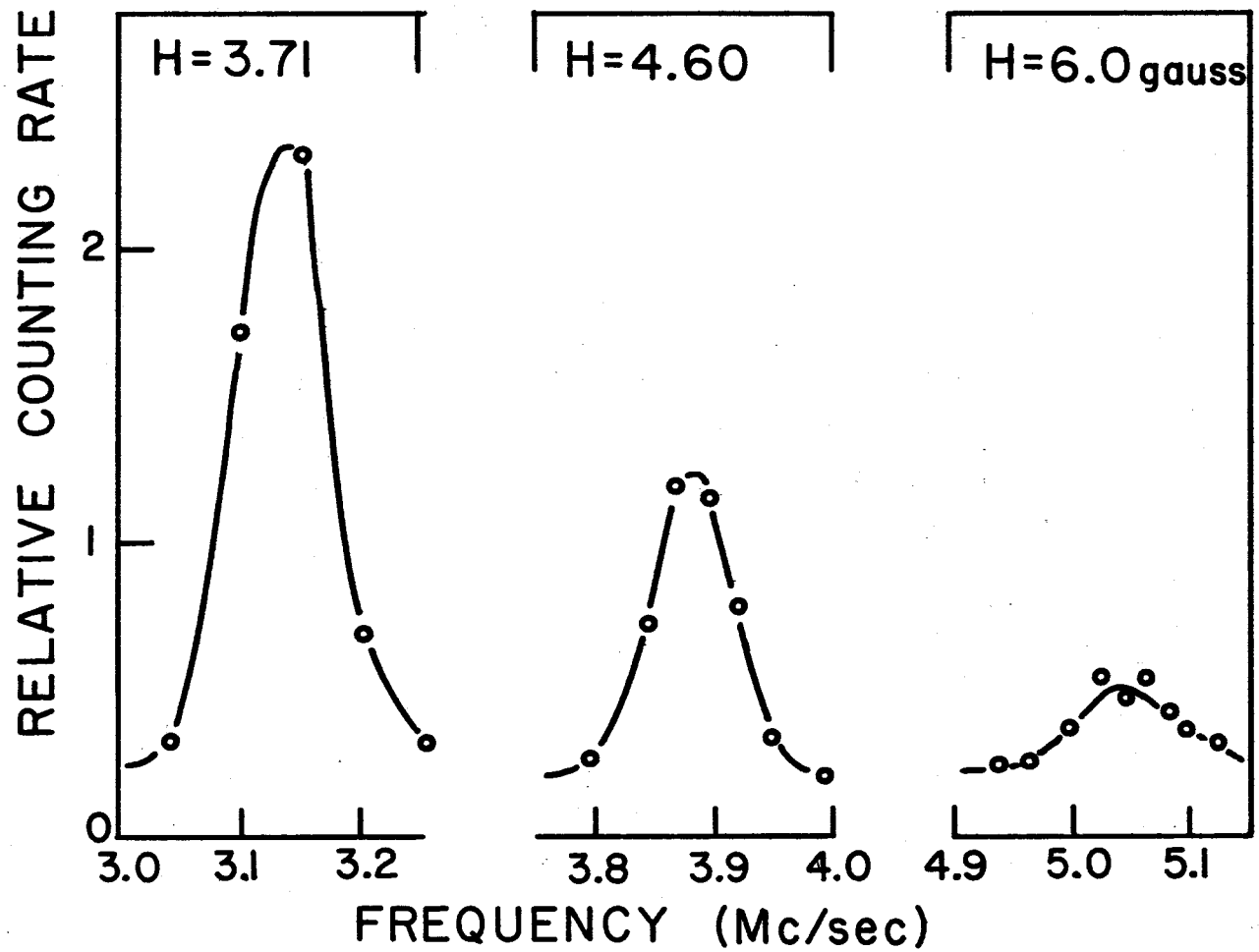
H=3.71
H=4.60
H=6.0 gauss
RELATIVE COUNTING RATE
0
1
2
3.0
3.1
3.2
3.8
3.9
4.0
4.9
5.0
5.1
FREQUENCY (Mc/sec)

losing track of the resonances. In this context, even if a resonance were observed within the search range at a higher field, one would not know with which transition it should be identified.

It was first thought that the $J = 2$, $F = 5/2$ resonance could be investigated by a technique using two r.f. loops and two oscillators to excite the resonance in two steps. Unfortunately, even at 12 gauss, there were a pair of single oscillator resonances near its predicted position and the two oscillator effects could not be interpreted. Since the intensity and shape of the single oscillator resonances depended strongly on the r.f. power, a series of experiments was carried out to investigate this effect. In order to obtain consistent results, it was found necessary to reduce the power level to a minimum so that only two quantum resonances were observed.

Since the two oscillator experiment was not feasible and since the two resonances already observed at 12 gauss could not be identified, an extensive series of one oscillator experiments was carried out. Figure 14 is a composite spectrum of resonances taken at different times, all at 12 gauss. The resonances observed appeared in pairs, one more intense than the other and with different r.f. power dependence. This meant that the relative intensity could not be used as an aid in identification. Since spurious resonances had been observed on one or two occasions when the alignment of the slit system was slightly less than optimum, it was considered a possibility that only one member of each pair of resonances was a two quantum resonance. The other might be a one quantum transition of the type $m_J = 0 \rightarrow m_J \pm 1$ which should not be observable in an ideal flop-in machine. However, if the oven were off the beam axis, atoms in a state $m_J = 0$ could pass straight

Figure 14

Zeeman transitions observed in $Sm^{153}$ at 12.0 gauss. The short vertical lines along the frequency axis represent the nominal transition frequencies and the sloping lines indicate the frequency shift due to hyperfine interaction. The upper vertical segments indicate the frequencies calculated using the final values of the hyperfine interaction constants, $A_2 = -2.57$ Mc/sec and $B_2 = 306.5$ Mc/sec.

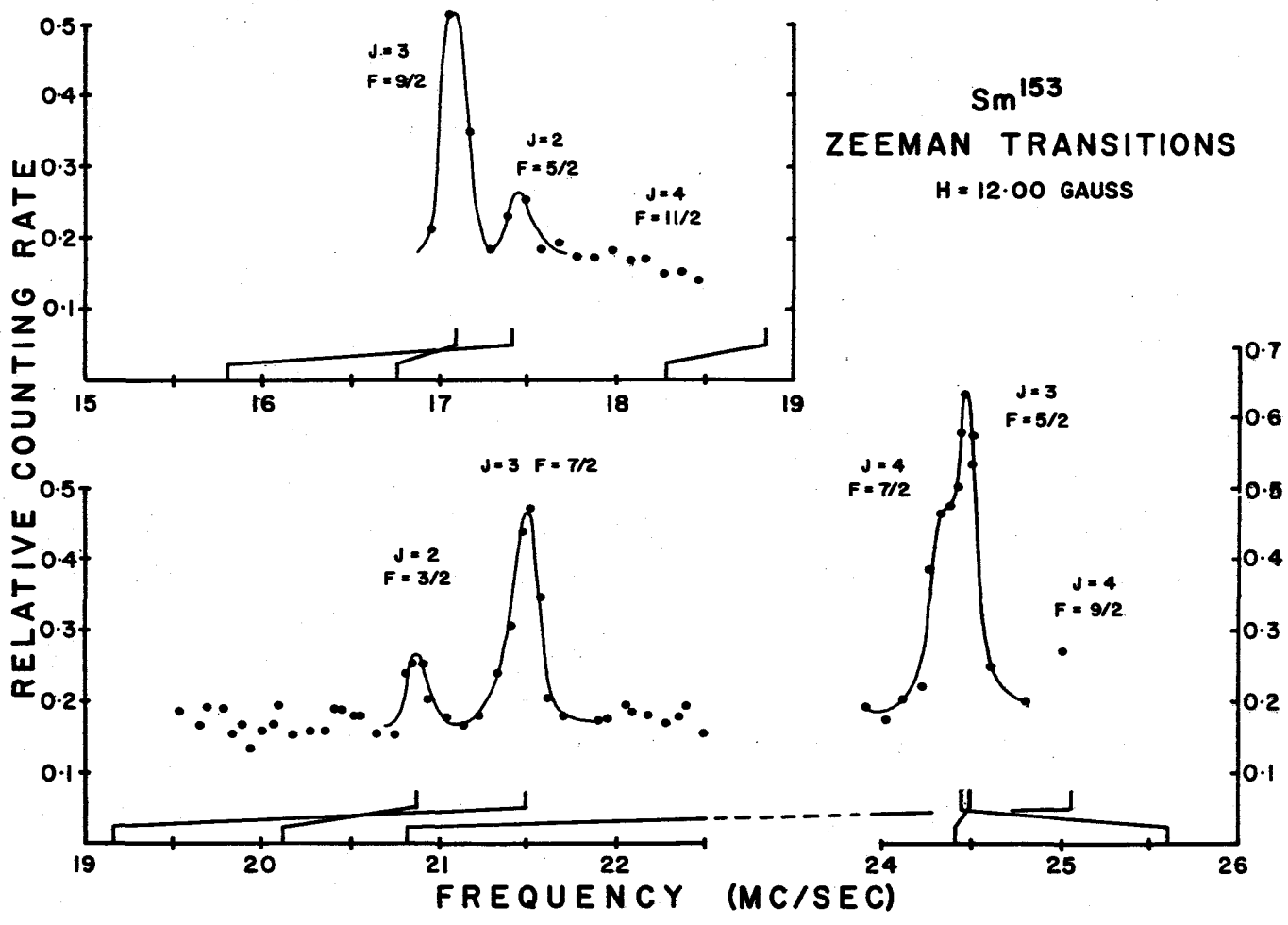
Sm153
ZEEMAN TRANSITIONS
H = 12·00 GAUSS
J = 3
F = 9/2
J = 2
F = 5/2
J = 4
F = 11/2
J = 3 F = 7/2
J = 2
F = 3/2
J = 3
F = 5/2
J = 4
F = 7/2
J = 4
F = 9/2
RELATIVE COUNTING RATE
FREQUENCY (MC/SEC)
0·5
0·4
0·3
0·2
0·1
0·7
0·6
15
16
17
18
19
20
21
22
24
25
26

through the A-magnet slit at an angle. Then, if they transferred to a state $m_J = \pm 1$ (the sign depending on the direction of the offset), they would deflect back toward the beam axis, miss the stop wire and, for a range of velocity and initial angle, reach the detector. Without velocity focussing this type of resonance would have low intensity. To clarify the situation a deliberate attempt was made to observe $J = 1$, $F = 3/2$ and $J = 2$, $F = 3/2$ resonances with the oven offset first in one direction and then in the other. Reference to Figures 1 and 2 shows that neither of these transitions corresponds to a conventional flop-in resonance since there are no $m_J = +1$ states for this value of F. No significant increase in counting rate was observed and we conclude that these resonances are not observable with this machine when it is correctly aligned. Thus all the resonances in Figure 14 must be normal multiple quantum transitions.

In order to fit the data, it was necessary to predict the spectrum for a wide range of values of the interaction constants. To do this accurately, the secular determinant of the magnetic interaction was solved; for $I = 3/2$ an analytical solution can be obtained for the subdeterminants, corresponding to different m, since the equations are quartic at most. Programs were written for the Bendix G15D computer for $J = 1, 2, 3$, and 4 to solve for the eigen values of $|Fm\rangle$. The output consisted of an array of these energies which were subtracted manually to give the transition frequencies. Solutions were obtained for discrete values of A and B for the desired range of B/A. The computation was performed in double precision (twelve-figure accuracy) and truncated at .0001 Mc/sec in the type-out. For a few cases, the computed results were checked by manual calculation and the errors were less than 1 kc/sec.

By comparing the observed frequencies with the computed values it was apparent that there is only one consistent way of identifying the six resonances shown in Figure 14. Figure 15 shows the ranges of $B_2$ and $A_2$ for which this assignment is possible. The width of each band reflects the experimental uncertainty of the corresponding resonance frequency. These bands all overlap in the general region of $|B| \approx 300$, $|A_2| \approx 3$ for $B/A < 0$. The $J = 4$, $F = 7/2$ resonance sets a very narrow limit on $|A|$ because this state is perturbed strongly by the adjacent $J = 4$, $F = 9/2$ hyperfine level. On the basis of these data, and with the assumption that the ratios $A_J/A_2$ and $B_J/B_2$ are not very different from those of $Sm^{147}$ and $Sm^{149}$, then

$$|A_2| = 2.85\ (40)\ \text{Mc/sec}$$

$$|B_2| = 303\ (5)\ \text{Mc/sec}$$

and $$B_2/A_2 < 0 \ .$$

These values of A and B were used to compute the predicted positions of the resonances at 3.68 and 12 gauss. These are shown in Figures 12 and 14 by the vertical bars. For comparison the nominal frequencies are shown also.

Although these values are sufficiently accurate for a calculation of the nuclear moments, it was felt that further experiments were required to make absolutely certain that this assignment was correct. Examinations of the Zeeman transitions at a higher field would have required a great deal of computer time in order to calculate the necessary frequencies. Instead, it was thought reasonable to search

Figure 15

The limits set on $|A_2|$ and $|B_2|$ by each of the resonances indicated in figure 14. Only values in the small shaded area for $B_2/A_2 < 0$ are consistent with all six resonances.

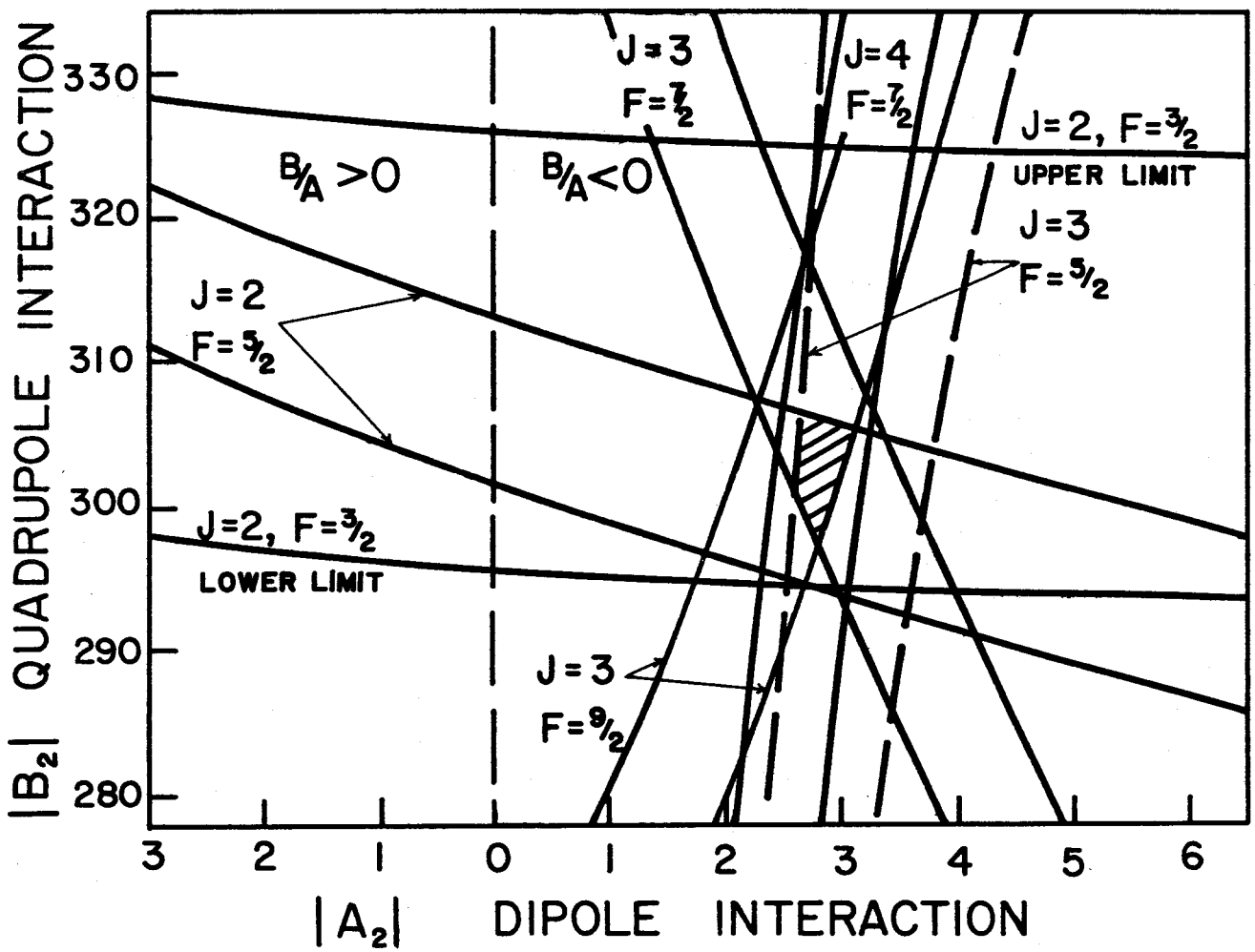
|B₂| QUADRUPOLE INTERACTION
330
320
310
300
290
280
3
2
1
0
1
2
3
4
5
6
|A₂| DIPOLE INTERACTION
B/A >0
B/A<0
J=3
F=7/2
J=4
F=7/2
J=2, F=3/2
UPPER LIMIT
J=3
F=5/2
J=2
F=5/2
J=2, F=3/2
LOWER LIMIT
J=3
F=9/2

for the direct hyperfine transitions. In addition, the direct observation would be independent of the ratios of the interaction constants.

b. The Direct Hyperfine Transitions

The interaction constants predicted above establish the ordering of all the hyperfine levels and the number and frequency of all transitions. In this case all eleven zero field hyperfine splittings are observable by single quantum flop-in transitions. In $J = 1$ state, for example, there are 3 $\pi$ components and 2 $\sigma$ components connecting the $F = 3/2$ and $F = 1/2$ states and one $\pi$ component between the $F = 3/2$ and $F = 5/2$ states. The $\pi$ components are illustrated in the right-hand portion of Figure 1. Between the $F = 11/2$ and $F = 9/2$ states of $J = 4$ there are two $\pi$ transitions. The remaining hyperfine structure separations are measurable by only one transition each. In summary, the 16 predicted transitions range in frequency from 8 to 650 Mc/sec.

The $J = 2$ $(5/2, 1/2 \leftrightarrow 3/2, 3/2)$ transition was investigated first since this $\pi$ transition is least sensitive to the relatively large uncertainty in B. This was observed within the predicted range and the experimental frequency used to correct the value of $A_2$ and $B_2$. These corrected values were then used to calculate the positions of the other direct transitions. Subsequently, all eleven different $\pi$ transitions were observed, and Figure 16 shows a typical resonance of this type. Also, four of the five possible $\sigma$ resonances were observed. The $J = 1$ $(1/2, 1/2 \leftrightarrow 3/2, 1/2)$ resonance was omitted since the separation between the $F = 1/2$ and $F = 3/2$ states was already determined by four different transitions. Figure 17 shows a typical $\sigma$ resonance. The dip in the centre is an interference effect (Cameron, 1962) and is

Figure 16

A $J = 1$ $(5/2,\ 3/2 \longleftrightarrow 3/2,\ 1/2)$ resonance in a field of 2 gauss. This is typical of the direct hyperfine $\pi$ transitions.

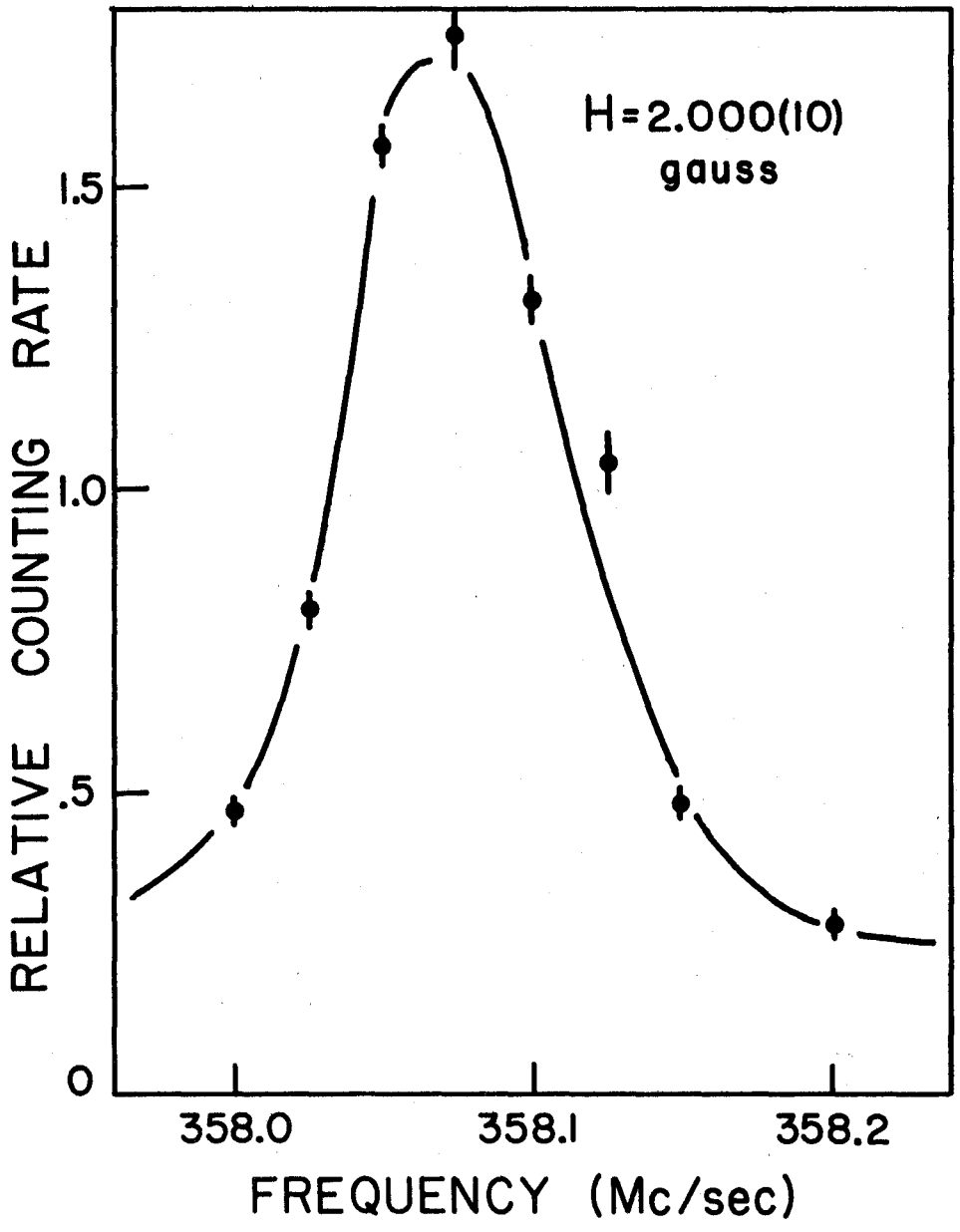
H=2.000(10)
gauss
1.5
1.0
.5
0
RELATIVE COUNTING RATE
358.0
358.1
358.2
FREQUENCY (Mc/sec)

Figure 17

A J = 2 (7/2, 1/2 $\longleftrightarrow$ 5/2, 1/2) resonance in a field of 1 gauss. This line shape with a central minimum is typical of $\sigma$ resonances observed with loop (b) shown in figure 6.

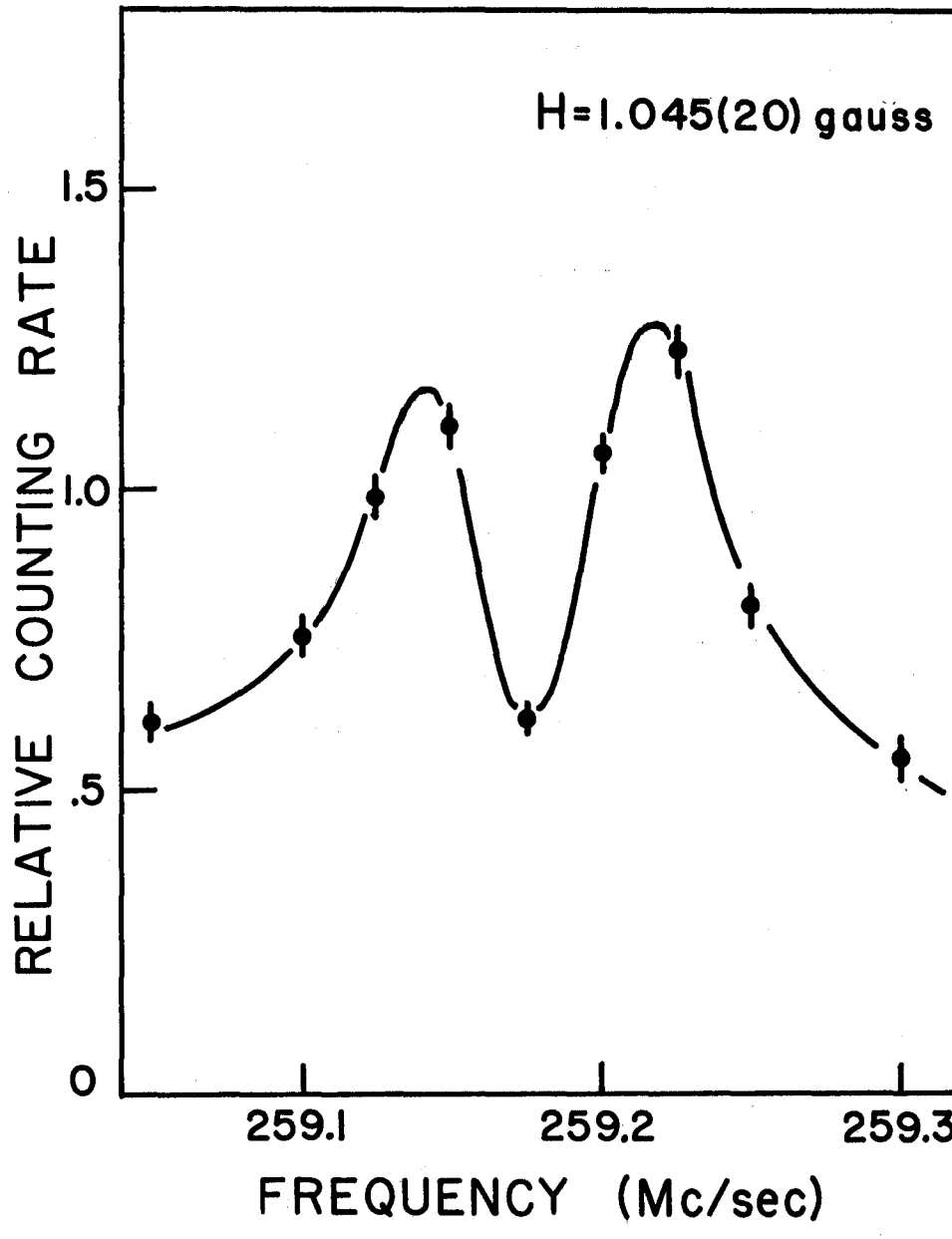
H=1.045(20) gauss
1.5
1.0
.5
0
RELATIVE COUNTING RATE
259.1
259.2
259.3
FREQUENCY (Mc/sec)

characteristic of the r.f. loop used (Figure 6b). It was observed only in the $\sigma$ resonances with low field dependence and in these cases permitted very precise location of the resonance frequency. For $\sigma$ transitions with large field dependence the effect is averaged out by the C field inhomogeneity.

Most of the resonances were observed at both 1 and 2 gauss and the frequencies are listed in Table VI. As a preliminary step these were corrected to zero field using perturbation theory. The zero field splittings were solved to give A, B, and C for each fine structure state. For J = 1 the octopole constant $C_1$ is identically zero, of course. The values of the interaction constants obtained in this way were then used to compute the exact field corrections. The final corrected values of the hyperfine separations and their averages are also shown in Table VI. These average values were used to solve for the values of A, B, and C in Table VII. Although only the relative signs of $A_J$, $B_J$, and $C_J$, for a given J, are determined by this process, the table lists the absolute signs determined by the method described below.

c. The Sign of $A_2$

The usual method of determining the sign of A, and therefore of $g_I$, is to examine the consistency between the data and the frequencies calculated with the term in $g_I$ included in the Hamiltonian. In the present case, however, A is unusually small -- so small, in fact, that $g_I$ is approximately $10^{-5}$ (in terms of the Bohr magneton). Since this is the same order as the uncertainty in $g_J$ to its present accuracy, the effect of $g_I$ on Zeeman frequencies is entirely negligible.

An alternative approach is necessary which depends on the fact that at intermediate magnetic fields the three levels in a double

TABLE VI

Direct Hyperfine Transitions in Samarium-153

| J | F | m | F' | m' | H gauss | $\nu_{observed}$ Mc/sec | $\nu_{H=0}$ Mc/sec | $\bar{\nu}_{H=0}$ Mc/sec |
|---|---|---|---|---|---|---|---|---|
| 1 | 3/2 | 3/2 | 3/2 | 1/2 | 2.000(10) | 358.070(15) | 356.068(35) | 356.054(12) |
| | 5/2 | 3/2 | 3/2 | 1/2 | 0.995(5) | 357.035(10) | 356.050(15) | |
| | 3/2 | -1/2 | 1/2 | -1/2 | 2.005(10) | 655.460(20) | 653.489(35) | |
| | 3/2 | -1/2 | 1/2 | -1/2 | 1.070(25) | 654.500(20) | 653.483(45) | |
| | 3/2 | -1/2 | 1/2 | 1/2 | 1.003(5) | 653.050(10) | 653.498(13) | 653.494(6) |
| | 3/2 | 1/2 | 1/2 | -1/2 | 1.003(5) | 653.880(10) | 653.487(12) | |
| | 3/2 | 1/2 | 1/2 | -1/2 | 1.017(5) | 653.900(10) | 653.501(12) | |
| | 3/2 | -3/2 | 1/2 | -1/2 | 1.017(10) | 655.025(15) | 653.494(30) | |
| 2 | 7/2 | 1/2 | 5/2 | 1/2 | 1.045(20) | 259.180(10) | 259.206(11) | 259.200(7) |
| | 7/2 | 1/2 | 5/2 | 1/2 | 2.000(5) | 259.215(10) | 259.194(10) | |
| | 5/2 | 1/2 | 3/2 | 3/2 | 1.970(10) | 201.830(20) | 198.018(40) | |
| | 5/2 | 1/2 | 3/2 | 3/2 | 1.015(15) | 199.960(25) | 198.036(55) | 198.002(30) |
| | 5/2 | 1/2 | 3/2 | 3/2 | 2.012(15) | 201.825(15) | 197.932(45) | |
| | 3/2 | -3/2 | 1/2 | -1/2 | 1.010(15) | 272.500(15) | 272.073(22) | 272.073(15) |
| | 3/2 | -3/2 | 1/2 | -1/2 | 2.006(10) | 272.940(15) | 272.073(20) | |

TABLE VI (CONTINUED)

| J | F | m | F' | m' | H gauss | $\nu_{observed}$ Mc/sec | $\nu_{H=0}$ Mc/sec | $\nu_{H=0}$ Mc/sec |
|---|---|---|---|---|---|---|---|---|
| 3 | 9/2 | 1/2 | 7/2 | 1/2 | 0.955(15) | 110.300(10) | 110.297(11) | 110.299(9) |
| | 9/2 | 1/2 | 7/2 | 1/2 | 1.010(5) | 110.305(15) | 110.302(16) | |
| | 7/2 | 1/2 | 5/2 | 3/2 | 1.000(15) | 71.215(15) | 68.852(47) | |
| | 7/2 | 1/2 | 5/2 | 3/2 | 1.050(5) | 71.325(25) | 68.844(37) | 68.818(18) |
| | 7/2 | 1/2 | 5/2 | 3/2 | 1.000(5) | 71.160(15) | 68.797(27) | |
| | 7/2 | 1/2 | 5/2 | 3/2 | 2.040(10) | 73.845(20) | 68.819(47) | |
| | 5/2 | -1/2 | 3/2 | -1/2 | 1.020(5) | 131.590(20) | 132.256(24) | |
| | 5/2 | -1/2 | 3/2 | -1/2 | 1.000(5) | 131.650(15) | 132.303(19) | 132.286(15) |
| | 5/2 | -1/2 | 3/2 | -1/2 | 1.995(5) | 130.990(20) | 132.281(24) | |

TABLE VII

Hyperfine Interaction Constants for Samarium-153

| J | Dipole Interaction A (Mc/sec) | Quadrupole Interaction B (Mc/sec) | Octupole Interaction C (Mc/sec) |
|---|---|---|---|
| 1 | -2.100(5) | 289.042(4) | ——— |
| 2 | -2.573(6) | 306.521(21) | -0.0003(9) |
| 3 | -3.115(4) | 165.824(20) | -0.0087(12) |

Direct hyperfine transitions were also observed in the state J = 4. However, in this case, due to the uncertainty in the large field corrections, the values are not sufficiently consistent to be considered final.

quantum transition are not equally spaced. Normally one excites such a transition with the oscillator set at the mean of the two one-quantum frequencies. However, it can be induced in two stages using two separate oscillators, each set to excite one of the one-quantum transitions. In this case, if the different frequencies are applied to two different loops in the C-magnet (Figure 18) then the transitions can only go from upper state ($m_J = +1$) to lower state ($m_J = -1$) or vice versa depending on the order in which the frequencies are applied. Now, if an obstacle is placed in the B-magnet gap, as shown in Figure 18, it will act as a state selector passing only those atoms with positive $m_J$ in that magnet. Thus, only atoms undergoing a transition to this state will be detected. The order of the frequencies which can produce a resonance under these conditions depends on the sign of A.

It was necessary to pick a field such that the two frequencies would be far enough from the mean position of any observable transition so that either frequency alone could not give a resonance. The computer routine was used to predict the spectrum at several fields and at 25 gauss it was found that the $J = 2$, $F = 3/2$ resonance would be suitable. Figure 19 shows the energy levels essential to this resonance for $A_2$ assumed negative and positive. Since the terms in $g_I$ are negligible, the only difference between these is that the diagram is inverted. The same two frequencies are involved in each case but if $A_2$ is negative the lower frequency must be applied to the first loop in order to produce an observable transition. If $A_2$ is positive, the reverse holds true.

The experiment was carried out by first observing the effects of only one frequency at a time on first one loop (1) and then the other (2) to make sure that individually they had no effect. Then both loops were

Figure 18

A plan view of the atomic beam apparatus showing the two r.f. loops and stop used to determine the sign of $A_2$. The stop S acts as a state selector in the B-magnet passing only atoms with $m_J > 0$.

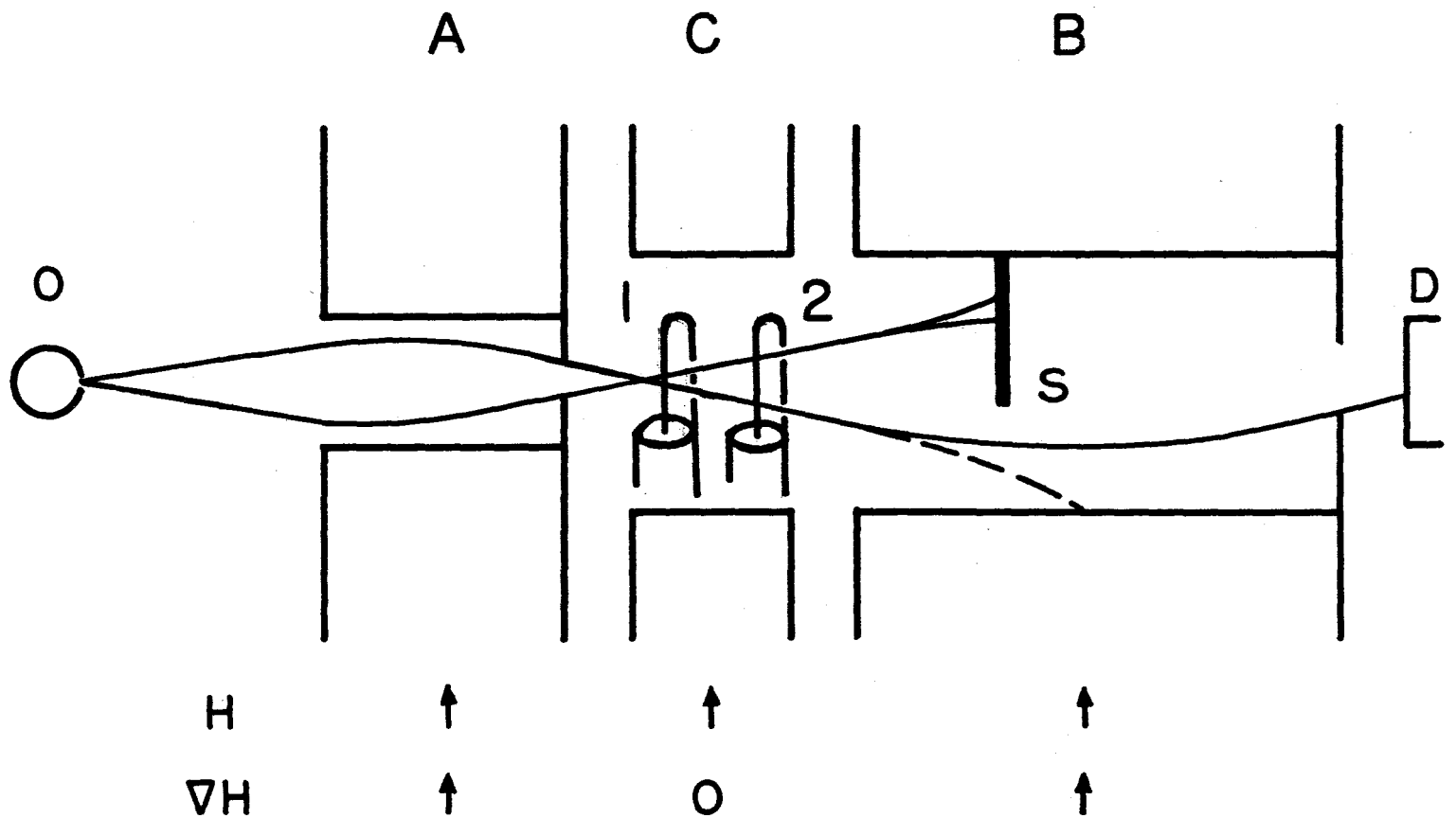
A
C
B
O
1
2
S
D
H
∇H
O

Figure 19

The results of a two oscillator experiment at 25 gauss to determine the sign of $A_2$ are plotted in the lower portion of the diagram. The solid points are the counting rates observed with two oscillators, each set at the frequency appropriate for exciting half of the two quantum jump. They are plotted against the average frequency $(\frac{\nu_1 + \nu_2}{2})$ in the left-hand diagram for $\nu_1 < \nu_2$ and in the right-hand diagram for $\nu_1 > \nu_2$. The corresponding $J = 2$, $F = 3/2$ energy levels are shown above. The single oscillator points taken for reference are plotted as open circles at the same abscissa as the corresponding two oscillator point.

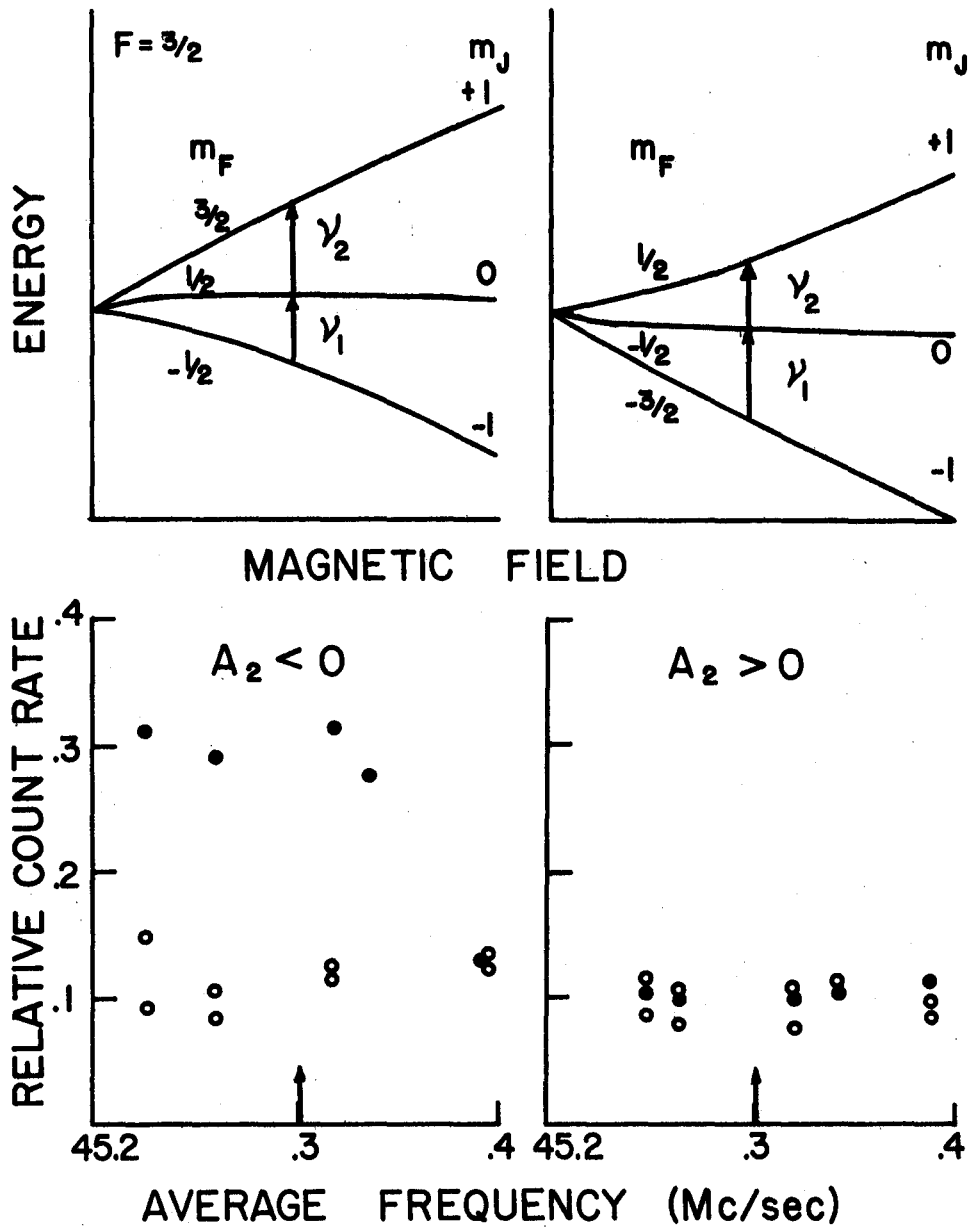
F = 3/2
$m_J$
+1
$m_F$
3/2
1/2
-1/2
$\nu_2$
$\nu_1$
0
-1
ENERGY
$m_J$
+1
$m_F$
1/2
-1/2
-3/2
$\nu_2$
$\nu_1$
0
-1
MAGNETIC FIELD
RELATIVE COUNT RATE
.4
.3
.2
.1
$A_2 < 0$
$A_2 > 0$
45.2
.3
.4
45.2
.3
.4
AVERAGE FREQUENCY (Mc/sec)

excited simultaneously, first with the lower frequency on loop 1 and the higher frequency on loop 2 and then in the reverse order. This was repeated several times for frequencies close to those calculated and the results are plotted in Figure 19. The points for two oscillators are plotted against $\bar{\nu}$, the average frequency, and the corresponding points with only one oscillator are plotted at the same abcissa. In the left-hand figure, the lower frequency was applied to loop 1 and the higher to loop 2 so that this case corresponds to $A_2$ negative. In the right-hand figure, the frequencies were reversed, corresponding to $A_2$ positive. The two-oscillator points in the right-hand figure and all the one-oscillator points have the same counting rate which corresponds to the machine background. However, the two-oscillator points in the left-hand figure are considerably higher, indicating that $A_2$ is negative.

One could conceivably carry out similar experiments to determine the sign of A in each fine structure state. This is hardly necessary since one such measurement serves to fix the sign of the magnetic moment. Furthermore, the interaction constants calculated for Russell-Saunders coupling are sufficiently accurate to determine the sign of the other $A_J$ relative to $A_2$.

## CHAPTER VI. DISCUSSION OF RESULTS

### 1. The Nuclear Spin of Samarium-155

The Zeeman resonances observed in the study of $Sm^{155}$ prove that the spin is 3/2. This measurement substantiates the spin assignment made on the basis of β-decay systematics (Schmid and Burson, 1959; Sund, Arns and Weidenbeck, 1960). Figure 20 shows the decay scheme of this nucleus based on their data. The lifetimes of the excited states of $Eu^{155}$ have also been measured and the inferred multipolarity of the γ-rays is consistent with this scheme (Vergnes and Jastrzebski, 1961). The spin assignments of the europium states are also consistent with the conversion coefficients and angular correlation of the γ-rays. However, the analysis relies on the assumed spins of the $Sm^{155}$ and $Eu^{155}$ ground states. The present result confirms these assumptions. The ground state of samarium can then be identified with two Nilsson odd-neutron energy levels, either (521) 3/2 - or (651) 3/2 +. The former state is more probable because no β-decay between ground states has been observed. In this case its absence would follow from the hindering of the transition according to the selection rules proposed for deformed nuclei (Alaga, 1955). In the other case no such ready explanation exists. The Nilsson energy level corresponding to the ninety-third neutron is emphasized for clarity in Figure 21. This shows that in the region where the ground state spin of $Sm^{155}$ would be 3/2 -, the nucleus would have large deformation ( $\delta > 0.3$) or small deformation ($\delta \approx 0.2$).

Figure 20

The decay schemes of $Sm^{155}$ and $Sm^{153}$. The energy of the $\beta$-rays are given in Mev and the reduced lifetimes (log ft) are given in the brackets. Some of the europium states are labelled with the Nilsson assymptotic quantum numbers ($Nn_z\Lambda$).

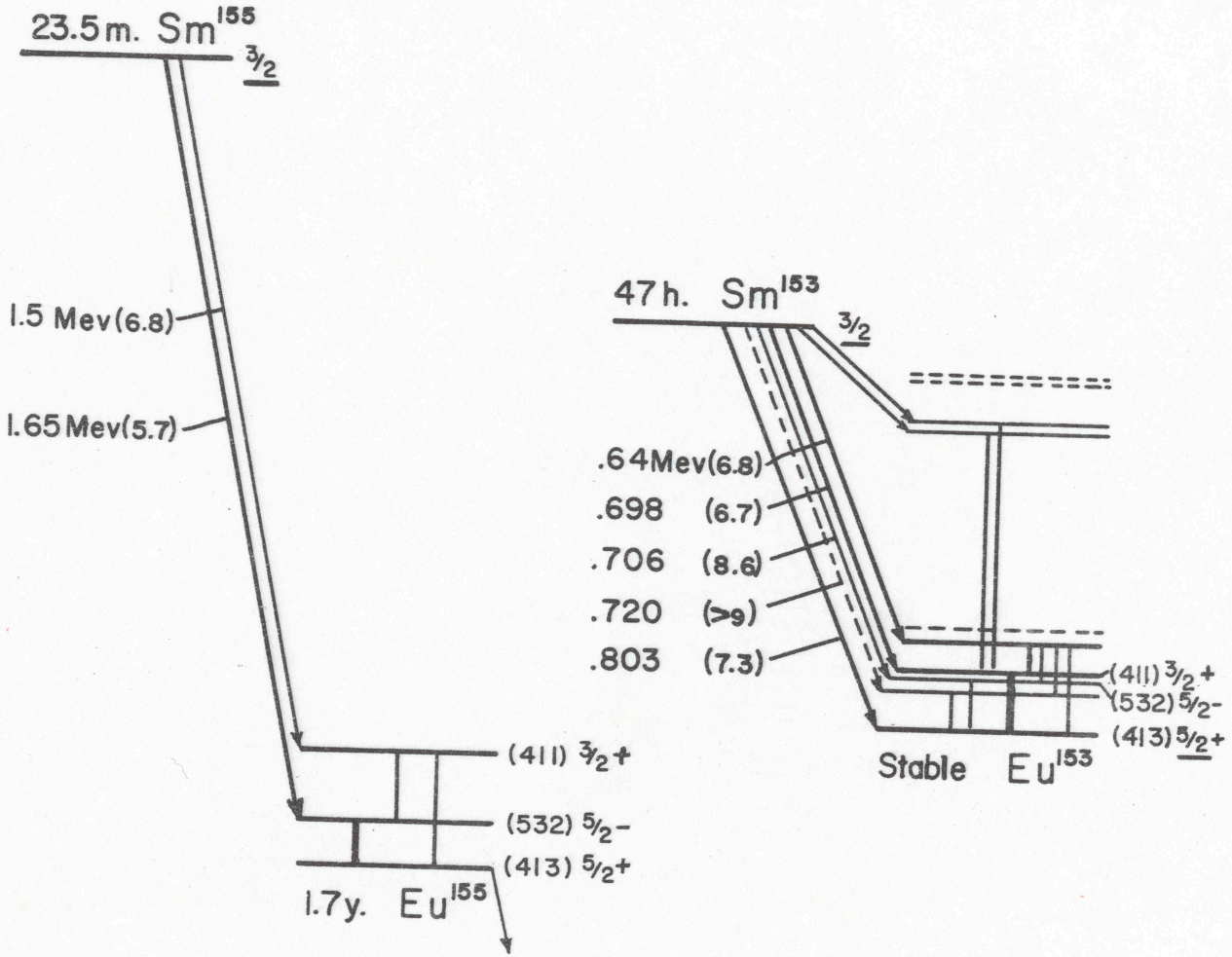
23.5 m. Sm155
3/2
1.5 Mev(6.8)
1.65 Mev(5.7)
(411) 3/2+
(532) 5/2-
(413) 5/2+
1.7y. Eu155
47 h. Sm153
3/2
.64 Mev(6.8)
.698 (6.7)
.706 (8.6)
.720 (>9)
.803 (7.3)
(411) 3/2+
(532) 5/2-
(413) 5/2+
Stable Eu153

Figure 21

The energy of odd neutron collective states are given as a function of deformation (Nilsson, 1955). The possible states for the 91st neutron are indicated by the dots while those of the 93rd neutron are marked by the heavy line.

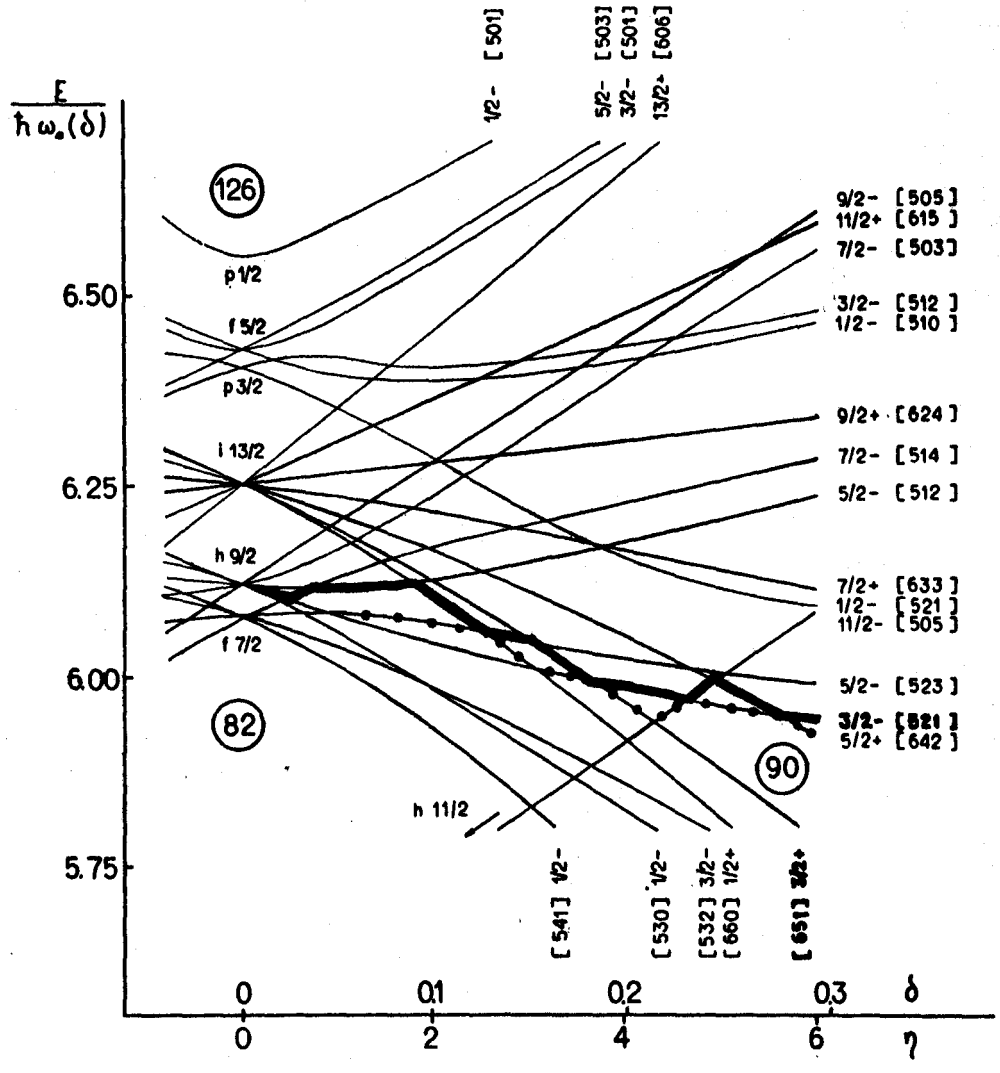
E / ħω₀(δ)
6.50
6.25
6.00
5.75
126
82
90
p 1/2
f 5/2
p 3/2
i 13/2
h 9/2
f 7/2
h 11/2
1/2- [501]
5/2- [503]
3/2- [501]
13/2+ [606]
9/2- [505]
11/2+ [615]
7/2- [503]
3/2- [512]
1/2- [510]
9/2+ [624]
7/2- [514]
5/2- [512]
7/2+ [633]
1/2- [521]
11/2- [505]
5/2- [523]
3/2- [521]
5/2+ [642]
[541] 1/2-
[530] 1/2-
[532] 3/2-
[660] 1/2+
[651] 3/2+
0
0.1
0.2
0.3
δ
0
2
4
6
η

2. The Hyperfine Interaction Constants of Samarium-153

The interaction constants calculated from the zero field hyperfine separations are shown in Table VI with the signs derived from $A_2$. These results have not been corrected for perturbation by neighbouring fine structure states. In the worst case, J = 1, this correction is liable to shift the hyperfine levels by about 40 kc/sec. However, Schwartz has shown that the shifts must leave the value of the dipole interaction constant, A, unchanged (Schwartz, 1955). The perturbation terms off-diagonal in J are proportional to $\mu_I^2$, $\mu_I \cdot Q$ and $Q^2$. Because $\mu_I$ is small in this case, the correction in B should be negligible. In the other fine structure states the shifts will be smaller; however, the change in the octupole constant, C, may be an order of magnitude. Since neither this correction nor the relation between C and the nuclear octupole moment is available in the literature, for multi-electron atoms, it was impractical to do anything further with the octupole interaction.

The ratios of the constants for the various fine structure states are shown in Table VIII. For comparison, the measured values for $Sm^{147}$ and $Sm^{149}$ and those calculated for pure L-S coupling are also included. If the nucleus were a point, the ratios for the three isotopes would be the same. However, for a nucleus of finite size, they might differ because of a hyperfine anomaly. For f electrons this effect should be extremely small and in taking ratios only the difference between such anomalies is involved. This is borne out by the experimental ratios in the table, the differences being only slightly larger than the experimental errors. The relative errors for $A_J/A_2$ in $Sm^{153}$ are quite large because the A's are so small.

TABLE VIII

Comparison of Hyperfine Constant Ratios

| | $Sm^{147}$ (After Woodgate) | $Sm^{149}$ (After Woodgate) | $Sm^{153}$ (This Experiment) | L-S Coupling Calculated |
|---|---|---|---|---|
| $A_1/A_2$ | 0.81342(5) | 0.81332(3) | 0.81607(370) | 0.93750 |
| $A_3/A_2$ | 1.219841(8) | 1.219898(8) | 1.21075(440) | 1.09375 |
| $A_4/A_2$ | 1.44977(24) | 1.44966(8) | † | 1.21875 |
| $B_1/B_2$ | 0.94334(16) | 0.94256(28) | 0.94298(8) | 0.95455 |
| $B_3/B_2$ | 0.541398(85) | 0.54090(30) | 0.54099(10) | 0.53030 |
| $B_4/B_2$ | (-)0.33946(276) | (-)0.33957(610) | † | -0.34711 |

† Tentative values of the ratios for $Sm^{153}$, $J = 4$, are in agreement with Woodgate's ratios.

The values derived assuming L-S coupling (equation (14)) are quite close in the quadrupole case but differ by 10 - 20 % in the dipole case. This is an indication that the electron wave functions are not pure $^7F$. Conway and Wybourne have calculated the extent of intermediate coupling and configuration mixing which gives the correct fine structure spacing and $g_J$ values for the rare earths including samarium. They find admixtures of up to 5 % of other wave functions in the various fine structure states (Conway and Wybourne, 1963).

3. <u>The Nuclear Moments of Samarium-153</u>

In order to evaluate the nuclear moments from the interaction constants, one can use equation (14). However, the value of $\langle 1/r^3 \rangle_{4f}$ is required. Various calculations of $\langle 1/r^3 \rangle$ for the rare earth ions have been made (Bleaney, 1955; Freeman and Watson, 1962). The values for neutral atoms are smaller because the extra electron sees a shielded nuclear charge. Lindgren has calculated $\langle 1/r^3 \rangle$ for both ions and atoms with an estimated accuracy of 5 % (Lindgren, 1962). Freeman and Watson point out that Lindgren has neglected configuration mixing and that his values and estimated error should be suspect (Freeman and Watson, 1962). They also state that polarization of the electron core by the nuclear moments (Sternheimer, 1952) can lead to different values of $\langle 1/r^3 \rangle_{\text{effective}}$ for dipole and quadrupole interactions and estimate that these might differ by up to 20 %. A comparison of the magnetic moment of $Sm^{147}$ derived from electron paramagnetic resonance data with the value obtained by optical hyperfine structure, in an excited electron state, suggests that Lindgren's value of $\langle 1/r^3 \rangle_{4f}$ for the $Sm^{+++}$ ion may be 25 % too large. A recent

determination of $\mu_{147}$ by atomic beam direct measurement verifies the value obtained from optical spectroscopy (Woodgate, 1963).

In the case of $4f^6\ {}^7F_J$, appropriate to samarium, equation (14) reduces to

$$A_J = \frac{\mu_I\ \mu_o}{h\ I} \quad \left\langle \frac{1}{r^3} \right\rangle_{4f} \left[ \frac{58 + J(J+1)}{90} \right]$$

Using Lindgren's value for the samarium atom, $\left\langle 1/r^3 \right\rangle_{4f} = 5.55\ a_o^{-3}$, and substituting our value for $A_1 = -2.10$ Mc/sec we find that $\mu_{153} = -0.018(5)$ n.m. Or using $A_2 = -2.57$ Mc/sec, $\mu_{153} = -0.020(5)$ n.m. An uncertainty of 25 % has been quoted to allow for the combined errors in $\left\langle 1/r^3 \right\rangle$ and in the assumption of pure **L-S** coupling.

An alternative approach which does not depend on the computed value of $\left\langle 1/r^3 \right\rangle$ is possible. The Fermi-Segrè formula relates the magnetic moments of two isotopes to the ratio of their interaction constants, measured in the same electronic state. Neglecting the possibility of a hyperfine anomaly, we can write

$$\frac{\mu_{153}}{\mu_{147}} = \frac{A^{153}}{A^{147}} \cdot \frac{I_{153}}{I_{147}}$$

Using $\mu_{147} = -0.79$ n.m. $\pm$ 3 %, $A_1^{147} = -33.5$ Mc/sec and $I_{147} = 7/2$ (Woodgate, 1963) and our value of $A_1^{153}$, it follows that

$$\mu_{153} = -0.021(1) \text{ n.m.}$$

To this accuracy, the same value is obtained in all four electronic states since the ratios of the interaction constants, $A_J/A_2$, were the same in both experiments. When the final results of Woodgate's direct measurement become available the uncertainty in the magnetic moment will be further reduced. The good agreement between this value and those

obtained above must result from a fortuitous cancellation of the error in $\left\langle 1/r^3 \right\rangle$ by that made in assuming L-S coupling.

In order to evaluate the quadrupole moment of samarium-153 we must rely on equation (14) since no direct measurement of Q can be made. Although this expression, for L-S coupling, is only approximately valid, at least the calculated ratios $B_J/B_2$ agree with the experimental values (Table VIII). Thus the dependence on J appears to be correct but this does not guarantee the accuracy of the complete expression. In the ground state of samarium, the quadrupole interaction constant reduces to

$$B_J = \frac{-e^2}{h} \; Q \quad \left\langle \frac{1}{r^3} \right\rangle_{4f} \left[ \frac{J(J^2 + J - 17)}{15(2J + 3)} \right]$$

Again using Lindgren's value for $\left\langle 1/r^3 \right\rangle_{4f}$ and substituting $B_1^{153}$ = 289 Mc/sec, we find that

$$Q_{153} = 1.1(3) \text{ barn.}$$

In view of the criticism of Lindgren's calculations, outlined above, it is possible that the quadrupole moment should be increased by up to 25 %. The error has been assigned with this in mind.

For convenient reference the nuclear spins, magnetic dipole moments and electric quadrupole moments of the odd-A samarium isotopes are listed in Table IX. The magnetic moments were derived using the Fermi-Segrè formula, Woodgate's value of $\mu_{147}$ and the appropriate interaction constants. The quadrupole moments were evaluated using Lindgren's $\left\langle 1/r^3 \right\rangle_{4f}$.

TABLE IX

Nuclear Spins and Moments of Samarium Isotopes

| | Neutron Number | Nuclear Spin | Magnetic Moment (n.m.) | Quadrupole Moment (barns) |
|---|---|---|---|---|
| $Sm^{147}_{85}$ | 85 | 7/2 | -0.79(3) | -0.23(6) |
| $Sm^{149}_{87}$ | 87 | 7/2 | (-)0.68(3) | (+)0.065(15) |
| $Sm^{151}_{89}$ | 89 | 3/2, 5/2, 7/2 | | |
| $Sm^{153}_{91}$ | 91 | 3/2 | -0.021(1) | +1.1(3) |
| $Sm^{155}_{93}$ | 93 | 3/2 | | |

## 4. Comparison of Samarium-153 with Nuclear Models

On the basis of the nuclear shell model $Sm^{147}$, $Sm^{149}$ and $Sm^{151}$ should have spin 7/2. This has been observed for the first two isotopes. No measurements have yet been made on $Sm^{151}$ but it is hoped that this will be done in the near future. $Sm^{153}$ and $Sm^{155}$ do not have the predicted shell model spin of 9/2; instead, they both have spin 3/2. This can be explained in the collective model. Referring to Figure 21, $Sm^{153}$ can be identified, on the basis of its spin alone, with either the collective state (521) 3/2- or (651) 3/2+. For 91 neutrons, the former state is predicted to be the groundstate for a nuclear deformation $\delta \approx 0.25$. Alternatively, for a smaller deformation $\delta \approx 0.18$, the state (651) 3/2+ is possible.

The observable electric quadrupole moment for a deformed nucleus can be calculated using equations 6 and 7. The upper portion of Figure 22 shows Q as a function of $\delta$ for I = 3/2. The observed value, 1.1 barns, corresponds to a deformation $\delta = 0.25$. Thus the quadrupole moment favours the assignment (521) 3/2-.

The magnetic moment predicted by the collective model, for an odd neutron nucleus, can be calculated from equation 5

$$\mu = \frac{I}{I+1}\left[g_R + \frac{1}{2} g_s \sum (\alpha^2_{\ell,\Omega-\frac{1}{2}} - \alpha^2_{\ell,\Omega+\frac{1}{2}})\right] .$$

This has been evaluated using $g_R \approx Z/A \approx 0.4$ for the states (651) 3/2+ and (521) 3/2- and the results are plotted in the lower part of Figure 22. For the deformation obtained from Q neither state is predicted to have a magnetic moment near the small observed value. Quenching the free neutron gyromagnetic ratio from -3.8 to -2 results in some improvement as shown but there is no precedent for such a drastic reduction

Figure 22

In the lower part of the figure magnetic moments calculated for the collective states (521) and (651) are compared with the experimental value for $Sm^{153}$. The upper diagram gives the dependence on deformation of the observable quadrupole moment of a spheroidal nucleus ($I = 3/2$) for comparison with the observed value.

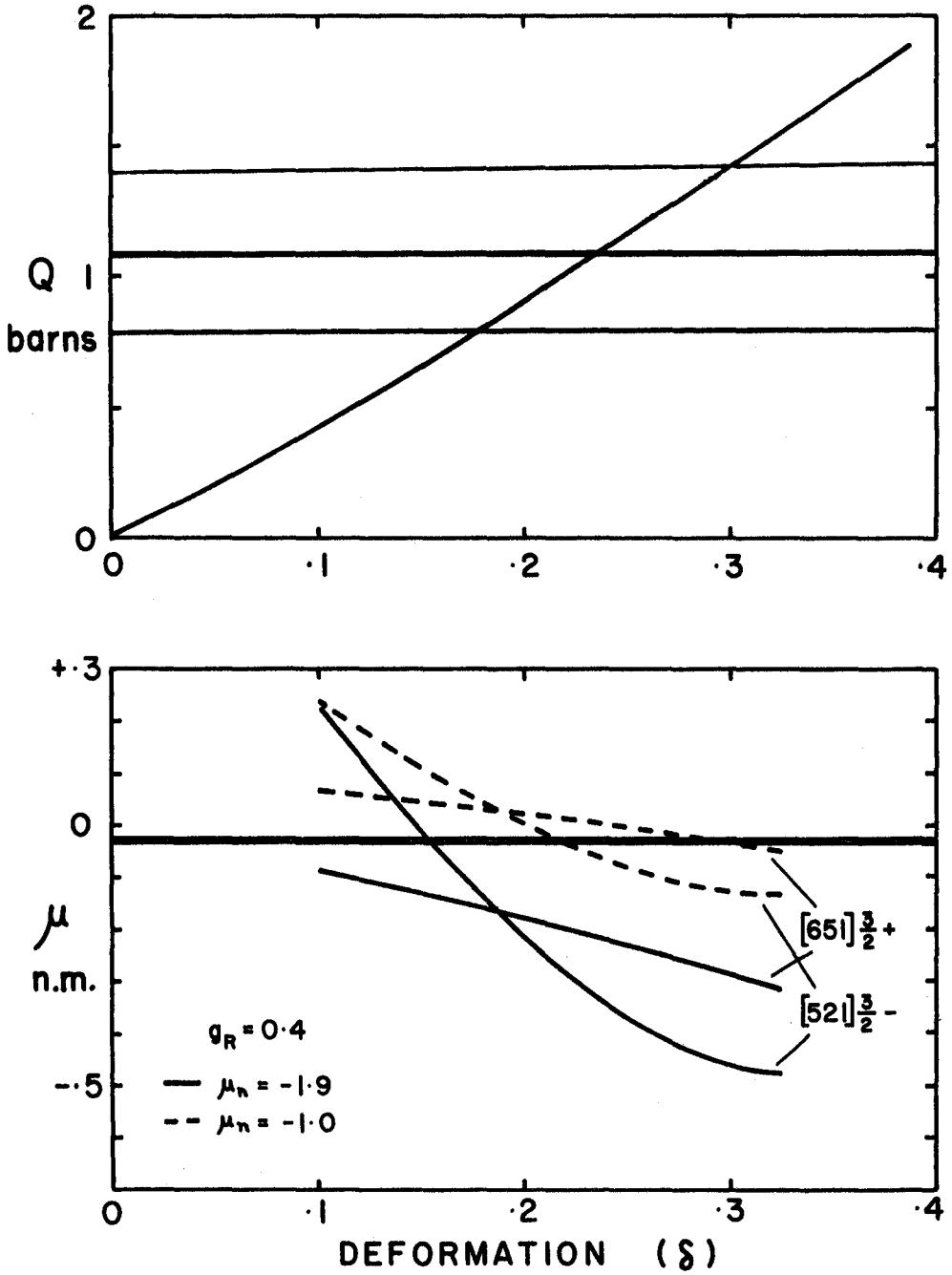
2
Q 1
barns
0
0
·1
·2
·3
·4
+·3
0
μ
n.m.
-·5
[651] 3/2 +
[521] 3/2 -
g_R = 0·4
μ_n = -1·9
μ_n = -1·0
0
·1
·2
·3
·4
DEFORMATION (δ)

in $g_s$. It is noteworthy that in the case of $Eu^{153}$, an odd proton nucleus, the Nilsson model fails to predict the experimental magnetic moment unless the free proton moment is very considerably quenched. Reducing $g_R$, of course, makes an even larger difference between theory and experiment, in both cases. A recent measurement on $Sm^{152}$ shows that $g_R = 0.351(25)$ (Bauer and Deutsch, 1961). Thus the assumption of a value larger than 0.4 for $Sm^{153}$ would be quite unreasonable.

Although the parity of $Sm^{153}$ is not determined by $\mu_I$, it has been established indirectly by β-decay systematics. The decay scheme was shown in Figure 20 (Suter et al., 1962). These facts should be noted. First there is a β-decay directly to the ground state of $Eu^{153}$ (log ft = 7.3). Second, the branch feeding the 97.5 kev level has log ft = 8.6 and the γ-ray de-exciting this level is electric dipole. The other important point is that the spin and magnetic moment of $Eu^{153}$ have been measured. The spin, 5/2, requires that the ground state be associated either with the Nilsson proton state (413) 5/2+ or (532) 5/2-. The latter is completely ruled out by the magnetic moment measurement. Therefore, the states must be identified as in the diagram. In this case the $Sm^{153}$ ground state must have negative parity in order to make the β-decay to the europium ground state first forbidden. One is forced to explain the large log ft value of the transition to the 97.5 kev level as being due to a change in nuclear deformation (Mottelson and Nilsson, 1959).

This decay scheme is significantly different from that of $Sm^{155}$ where the 1.65 Mev β transition to the analagous excited state of $Eu^{155}$ has log ft = 5.7 as compared with 8.6 and also there is no transition

to the ground state of $Eu^{155}$. This can be explained if the nuclear deformation of $Sm^{155}$ is about 0.2, corresponding to a state assignment (521) 3/2-, in which case there is no change in nuclear shape for the decay to the excited state (532) 5/2-. On the other hand, the decay to the ground state (413) 5/2+ is first forbidden, hindered, and now also involves a change in deformation.

Although the results of this investigation have elucidated some of the properties of $Sm^{153}$ and $Sm^{155}$, further studies, both experimental and theoretical, would be useful. Firstly, if the octupole interaction constants could be interpreted, it is possible that the octupole moment of $Sm^{153}$ would lead to an unambiguous parity assignment for that nucleus. Secondly, if more realistic Nilsson model calculations, including the effects of pairing force for example, were available, a comparison of the magnetic moments might be more fruitful. Thirdly, in order to verify the above explanation for the different decays of $Sm^{153}$ and $Sm^{155}$, it would be desirable to know more about the ground state properties of $Sm^{155}$ and $Eu^{155}$.

BIBLIOGRAPHY


Albertson, W. Phys. Rev. 47, 370 (1935)

Alpert, S. S. University of California Lawrence Radiation Laboratory Report UCRL 9850 (1961)

Arima, A. and Horie, H. Progr. Theoret. Phys. (Japan) 11, 509 (1954)

Baker, F. S. University of California Lawrence Radiation Laboratory Report UCRL 9364 (1960)

Bardeen, J., Cooper, L. N. and Schrieffer, R. Phys. Rev. 108, 1175 (1957)

Bauer, R. W. and Deutsch, M. Proceedings of the Rutherford Jubilee International Conference, Heywood, Manchester (1961)

Beavis, L. C. Sandia Corporation Technical Memorandum SCTM 256 A - 60 (14)(1960)

Bellamy, E. H. and Smith, K. F. Phil. Mag. 44, 33 (1953)

Besset, C., Horwitz, J., Messiah, A. and Winter, J. J. Phys. Rad. 15, 251 (1954)

Bilyaev, S. T. Kgl. Danske Vidensk. Selskab, Mat.-fys. Medd. 29, No. 16 (1959)

Bleaney, B. Proc. Phys. Soc. 68, 937 (1955)

Blin-Stoyle, R. J. Theories of Nuclear Moments. Oxford University Press, London (1957)

Bohr, A. and Mottelson, B. R. Kgl. Danske Vidensk. Selskab, Mat.-fys. Medd. 27, No. 16 (1953)

Breit, G. and Wills, W. A. Phys. Rev. 44, 470 (1933)

Brennan, M. H. and Bernstein, A. M. Phys. Rev. 120, 927 (1960)

Burke, D. G., Law, M. E. and Johns, M. W. Can. J. Phys. 41, 57 (1963)

Cabezas, A. Y., Lipworth, E., Marrus, R. and Winocur, J. Phys. Rev. 118, 233 (1960)

Cameron, J. A. Ph.D. Thesis, McMaster University (1962)

Cameron, J. A., King, H. J., Eastwood, H. K. and Summers-Gill, R. G. Can. J. Phys. 40, 931 (1962)

Casimir, H. B. G. On the Interaction Between Atomic Nuclei and Electrons. Teyler's Tweede Genootschap, Haarlem (1936)

Cohen, V. W., Moran, T. and Penselin, S. Phys. Rev. 127, 517 (1962)

Conway, J. G. and Wybourne, B. G. Phys. Rev. 130, 2325 (1963)

Elliot, J. P. and Flowers, B. H. Proc. Roy. Soc. A229, 536 (1955)

Freeman, A. J. and Watson, R. E. Phys. Rev. 127, 2058 (1962)

Gerlach, W. and Stern, O. Zeits. f. Physik 7, 249 (1921)

Goldring, G. and Scharenberg, P. P. Phys. Rev. 110, 701 (1958)

Goudsmit, S. Phys. Rev. 37, 663 (1931)

Hack, M. N. Phys. Rev. 104, 84 (1956)

Harmatz, B., Handley, T. H. and Mihelich, J. W. Phys. Rev. 128, 1186 (1962)

Haxel, O., Jensen, J. H. A. and Suess, H. E. Naturwiss. 35, 376 (1948)

Hubbs, J. C., Marrus, S., Nierenberg, W. A. and Worcester, J. L. Phys. Rev. 109, 309 (1958)

Kellogg, J. B., Rabi, I. I., Ramsey, N. F. and Zacharias, J. R. Phys. Rev. 55, 728 (1939); 57, 677 (1940)

King, A. S. J. Astro. Phys. 82, 140 (1935)

King, H. J. Ph.D. Thesis, McMaster University (1960)

Kisslinger, L. S. and Sorensen, R. A. Kgl. Danske Vidensk. Selskab, Mat.-fys. Medd. 32, No. 9 (1960)

Kisslinger, L. S. and Freed, N. Nuclear Phys. 25, 611 (1961)

Kopfermann, H. Nuclear Moments (trans. E. E. Schneider, Academic Press, New York)(1958)

Kurath, D. Phys. Rev. 101, 216 (1956)

Lindgren, I. Nuclear Phys. 32, 151 (1962)

Manning, G. and Rogers, J. Nuclear Phys. 19, 675 (1960)

Mayer, M. Phys. Rev. 74, 235 (1948)

Mottelson, B. R. and Nilsson, S. G. Kgl. Danske Vidensk. Selskab, Mat.-fys. Skr. 1, No. 8 (1959)

Nilsson, S. G. Kgl. Danske Vidensk. Selskab, Mat.-fys. Medd. 29, No. 16 (1955)

Nilsson, S. G. and Prior, O. Kgl. Danske Vidensk. Selskab, Mat.-fys. Medd. 32, No. 16 (1961)

Nordheim, L. Revs. Mod. Phys. 23, 322 (1951)

Paul, F. W. Phys. Rev. 49, 156 (1936)

Pichanick, F. M., Sandars, P. G. H. and Woodgate, G. K. Proc. Roy. Soc. 257, 277 (1960)

Rabi, I. I., Zacharias, J. R., Millman, S. and Kusch, P. Phys. Rev. 53, 318 (1938)

Ramsey, N. R. Molecular Beams (Oxford University Press) London (1956)

Rarita, W. and Schwinger, J. Phys. Rev. 59, 463 (1941)

Sund, R. E., Arns, R. G. and Wiedenbeck, M. L. Phys. Rev. 118, 776 (1960)

Savage, W. R., Hudson, D. E. and Spedding, F. H. J. Chem. Phys. 30, 221 (1959)

Schmid, L. S. and Burson, S. B. Phys. Rev. 115, 447 (1959)

Schmidt, T. Z. Physik 106, 358 (1937)

Schwartz, C. Phys. Rev. 97, 380 (1955)

Suter, T., Reyes-Suter, P., Gustaffson, S. and Marklund, I. Nuclear Physics 29, 33 (1962)

Vergnes, M. and Jastrzebski, J. J. Phys. Radium 22, 669 (1961)

Winocur, J. University of California Lawrence Radiation Laboratory Report UCRL 9174 (1960)

Woodgate, G. K. Proc. Roy. Soc. 263, 89 (1961)

Woodgate, G. K. (Oxford) Private Communication (1963)